UNIVERSITAT POLITÈCNICA
DE CATALUNYA
BARCELONATECH

Vrije
Universiteit
Brussel

Broadband Electrical Impedance Spectroscopy for dynamic Electrical Bio-Impedance characterization

Thesis for the degree of Doctor of Philosophy

by

Benjamin Sanchez Terrones

Supervisors: Dr. Ramon Bragós Bardia and Dr. Gerd Vandersteen

October 18, 2011

This page intentionally left blank.

Acknowledgements

First and foremost, the author is deeply indebted to Dr. Ramon Bragós and Dr. Gerd Vandersteen, for their continuous help, assistance and contribution to the technical development of this thesis. Their unconditional participation, support and guidance has encouraged me to perform the research work presented in this thesis. I honestly feel privileged to have had the opportunity to learn and work under your supervision. It has really been an honor and a pleasure.

This research is the result of the many collaborative work of several researchers from different areas. I would like to express my most sincere gratitude to Prof. Johan Schoukens, for giving me the opportunity to be with you and also the rest of your group from the ELEC department at Vrije Universiteit Brussels (VUB). Thank you for providing me constructive feedback and helpful answers to all of my questions.

Part of the research work done during the thesis has been possible due to the contributions of many medical and clinical staff from the different groups and hospitals. My gratitude to Dr. Carlos E. Semino for hosting me at the Tissue Engineering Laboratory from the Institut Quimic de Sarria (IQS) research group whenever I wanted. Thank you Carlos, for being a good friend. I really enjoyed the crazy talks during the lunch. I want to express you my gratitude for giving me the opportunity to work together with the Charlie's angels, Mar Torres, Teresa Muinos, Cristina Castells, Mireia Alemany, Nuria Marí and Verónica Puig. I have had a lot of fun working with all of you on such a great project.

I would like to express my gratitude to Dr. Antoni Bayes and people from Insuficencia Cardiaca i Regeneracio Cardiaca group (ICREC) at Fundacio d'Investigacio en Ciencies de la Salut Germans Trias i Pujol (IGTP).

I would also like also to express my gratitude to the medical and clinical staff from the Pneumology and Cardiology service from Hospital Santa Creu i Sant Pau (HSCSP) for giving me the opportunity to carry out part of the experimental work, which has been essential to give the existence and sense of this thesis. I am grateful to Dr. Alfons Torrego and Dr. Juan Cinca for the help and assistance during the experimental part.

The time during the thesis was made enjoyable in large part due to the many friends that became a part of my life. After four years, I have had the chance to meet many nice people who have helped me in one way or another to succeed with my thesis. I am especially grateful to Prof. Xavier Rosell for giving me the opportunity to take part of the Instrumentation and Biomedical Group research group. I cannot forget to mention Pere J. Riu, Juan Ramos, Miguel Ángel, Mireia Fernández, Lexa Nescolarde, Ferran Silva, Eva Vidal, Alfonso Mendez, Giuseppe Giovinazzo, Paco Bogonez, Andreu Atienza, Marc Pous, Marc Aragon, Ricardo Jauregui, Aleix Guasch, Hadis Mahdavi, Raul Macías, Noelia Rodríguez, Adolfo Benitez, Pau Juan, Josep Maria, Robert Matthews, Luis M. Vela, Ignasi Saladrigas (fellow of innumerable hardships to bike and on foot), Adrià Botifoll and Tomeu Palmer, all of them for the nice time we had together.

Last, I would like to thank my family for all their love and encouragement. To my parents, Águeda and Juan, who raised me with love and supported me in all my pursuits. My gratitude to our recently deceased colleague Orton. To my elder brother and his wife, Juan and Gemma, and to my lovely little sister, Sofia, all of them for being there when I needed them most.

And most of all for my loving, supportive, encouraging, and patient Iris, whose faithful support during the Ph.D. is so appreciated. You are everything to me. I love you darling.

Benjamín Sánchez Terrones

October 18, 2011

Abstract

Electrical Impedance Spectroscopy field has been widely used in clinical and biotechnological applications for the electrical characterization of a wide range of materials. When applied to biological materials, Electrical Bio-Impedance (EBI) provides information the tissue viability and cell morphology as well as cell membranes and intra/extra cellular spaces. The new Electrical Impedance Spectroscopy (EIS) techniques based on broadband excitations are expected to help to understand various unsolved problems in biomedical applications. Novel experiments that were thought to be difficult to perform in the past years were explored in order to solve complex problems encountered during the studies of time-varying biological systems, i.e. respiratory and cardiovascular systems.

The topics research presented in this thesis cover the challenges to measure time-varying EBI when exciting with broadband signals. On one hand, the optimal multisine excitation has been designed to overcome the intrinsic loss of accuracy when measuring in a reduced measuring time. More precisely, this research activity has contributed to a formal approach for designing the optimal time and frequency domain multisine excitation in such way that maximum accuracy is obtained when measuring with time and energy constraints. The results obtained have helped to understand how the multisine amplitudes and its frequency distribution contribute to increase the impedance spectrum accuracy.

On the other hand, reducing the measuring time makes the measurements to be prone to the influence of the transients introduced by noise and the dynamic time-varying properties of the system under test. While reducing the measuring time enables to measure the system non-stationary behavior, the low excited frequencies are prone to be corrupted by the leakage influence because of the

transients. For that reason, a novel frequency domain approach for impedance spectrum estimation has been applied by means of the Local Polynomial Method (LPM), which overcomes the signal processing limitations of current spectral estimation methods based on cross and auto correlation using windows.

This thesis has contributed with novel findings of relevance from successful applications where the optimal multisine excitation and the fast LPM has been together put in practice: (1) *in-vivo* human lungs tissue characterizaton, and (2), *in-vivo* healthy myocardium tissue electrical impedance characterization, both measurement campaigns with the collaboration of the pneumology and cardiology services from Hospital Santa Creu i Sant Pau (HSCSP).

Preface

This research work has been performed in the academic institution Technical University of Catalonia (UPC) and part of the tasks have been done in the ELEC Department from Vrije Universiteit Brussel (VUB).

The daily basis of this research work has been carried out in collaboration with the research group Insuficencia Cardiaca i Regeneracio Cardiaca (ICREC) from Fundacio d'Investigacio en Ciencies de la Salut Germans Trias i Pujol (IGTP), the Tissue Engineering Laboratory from Institut Quimic de Sarria (IQS) and the pulmonary and cardiology services from the Hospital de la Santa Creu i Sant Pau (HSCSP).

This research work has been mainly supported through the research grants from the Spanish Ministry MICINN SAF2008-05144-C02-02, Fundació La Marató TV3 080331, Redes de Investigación del Instituto de Salud Carlos III (REDINSCOR), by the 7FP-EU Regeneration of Cardiac Tissue Assisted by Bioactive Implants (RECATABI) European Project, by the Fund for Scientific Research (FWO-Vlaanderen), by the Flemish Government (Methusalem), and by the Belgian Government through the Interuniversity Poles of Attraction (IAP VI/4) Program.

This page intentionally left blank.

Contents

This page intentionally left blank.

Why don't you take a holiday Baldrick .... did you enjoy it?.

-Blackadder (1983)

0 Thesis Introduction

0.1 Research Projects

This thesis presents the results of the author's research work carried out during his PhD study in the Electronic and Biomedical Instrumentation Group at the Department of Electronics Engineering from the Technical University of Catalonia (UPC) in Barcelona (Spain). As wells as in the Department of Fundamental Electricity and Instrumentation (ELEC) from the Vrije Universiteit Brussels (VUB) in Brussels (Belgium). During these years, the author has been enrolled in three research projects financed by public funding. The goals of each of these projects are listed below:

- *Development of non-destructive monitoring techniques and minimally invasive cellular engineering applications for myocardial regeneration.* The objective of this project is to develop new techniques for *in-vitro* and *in-vivo* monitorization of cell cultures applied to cardiac regeneration. The project is carried out in collaboration with the Insuficència Cardíaca i Regeneració Cardíaca (ICREC) research group from Fundació d'Investigació en Ciències de la Salut Germans Trias i Pujol (IGTP). Funded by the Spanish Ministry MICINN through the research project SAF2008-05144-

C02-02.

- *Development of biological matrices to repair the postinfarction scar: Local release of stem cells, angiogenic factors and on-line myocardial regeneration monitoring.* The goal of this project is to regenerate infarcted myocardium with a novel bioactive implant based on electronic sensors, a porous biocompatible and biodegradable membrane and a local delivery of stem cells. The project is carried out in collaboration with the Insuficencia Cardiaca i Regeneracio Cardiaca (ICREC) research group from Fundació d'Investigació en Ciències de la Salut Germans Trias i Pujol (IGTP) and with the Tissue Engineering Laboratory from Institut Quimic de Sarria (IQS). Funded by Fundació La Marató TV3 through the research project 080331.

- *Regeneration of Cardiac Tissue Assisted by Bioactive Implants.* The objective of the project is to develop a patch to treat post-infarction damaged tissues and to promote remodeling of necrotic areas of the injured tissue. The project is carried out in collaboration with the Insuficència Cardíaca i Regeneració Cardiaca (ICREC) research group from Fundació d'Investigació en Ciències de la Salut Germans Trias i Pujol (IGTP). Funded by the 7FP-EU from the European Union.

The tasks developed for the previously mentioned projects have consisted in:

- Development of a system of combined electrical and mechanical training to promote stem cell differentiation.

- Development of the measuring techniques for *in-vitro* non-destructive monitoring of cell viability, proliferation and differentiation stages.

- Contribution to the implementation of a bioactive implant, consisting in a combination of scaffold, cells, electrodes and a measurement system to evaluate the engineered tissue viability for myocardium regeneration.

- Development of the methods for *on-line* dynamic engineered tissue characterization.

0.1.1 Introduction

The electrical impedance of a biological material is known as Electrical Bioimpedance (EBI) and it refers to the opposition that has a biological material to the pas-

sage of an electric current. The Electrical Bioimpedance enables to characterize physiological conditions and events that are interesting for physiological research and medical diagnosis. Although the Electrical Bioimpedance weakness is its dependence on many physiological parameters, it is a suitable approach for many medical applications where minimally invasive and real-time measurements with simple and practical implementations are needed.

The Electrical Impedance Spectroscopy (EIS) techniques based on broadband excitations are expected to help to understand various unsolved problems in biomedical applications. Broadband EIS opens up the possibility of reducing drastically the measuring time needed to measure EBI time-varying systems. However, measuring in a short time compromises the EBI accuracy. The way to overcome this intrinsic loss of accuracy relies on the design of the appropriate time/frequency input excitation properties and the use of suitable spectral analysis processing techniques.

The presented thesis covers the topics related to the study of broadband excitations for Impedance Spectroscopy in biomedical applications. More specifically, the influence of the multisine excitation time/frequency properties on the impedance spectrum accuracy and its further optimization. Furthermore, an state-of-art signal processing method has been implemented to process in real-time EBI data under the influence of transients, which is a common situation when measuring in a short measuring time. The main goal is to apply all this knowledge for myocardial tissue regeneration characterization. Nevertheless, any of the research projects that have supported this thesis have issued functional beating tissue at the moment of writing the thesis. For that reason, the theory presented has been validated over different dynamic EBI applications where the impedance spectrum non-stationary behavior was pretended to be characterized.

0.1.2 Thesis research objectives

The purpose of this research is to develop the methods for biological time-varying tissue characterization using Impedance Spectroscopy. This goal covers the following topics:

- Study, design and optimization of the broadband multisine excitation for Electrical Bio-Impedance characterization.

- Study of the non-parametric spectral analysis techniques for short time impedance spectrum estimation.

- Design, implementation and validation over a multichannel custom impedance analyzer system applied to non-destructive biological material characterization.

- Experimental validation of *in-vivo* myocardium tissue electrical impedance measurements.

- Development of tissue state multivariate estimators, including time-frequency behavior information, for *in-vitro* detection of stem cell differentiation and *in-vivo* heart tissue viability for cardiac tissue regeneration.

0.2 Thesis contents and outline

This PhD thesis is organized in two parts. The first part contains an introductory report to the research area of the thesis. The second part contains the manuscripts as a result of this research.

Part I is divided in five chapters that contain the main topics involved in the research activity performed during the thesis work. Chapter 1 is an introductory summary to the main concepts and definitions of the Electrical Impedance Spectroscopy (EIS) applied to Electrical Bioimpedance (EBI) measurements. Chapter 2 presents a comparative study of EIS using broadband signals and introduces the motivation for designing the optimal time-frequency excitation. At this point, the reader is recommended to read Paper A in order to go deeper into the optimal input excitation design. Chapter 3 examines the problem of estimating the impedance frequency response from short time measurements corrupted by the presence of transients. The reader is recommended to read Paper B to further examine its application for short time *in-vivo* myocardium tissue electrical impedance characterization. In Chapter 4 there is a clinical application where the findings of Chapter 2 and Chapter 3 have been put in practice for *in-vivo* human lung tissue characterization. Finally, Chapter 5 lists the major conclusions obtained in this thesis and the guidelines for future research.

Part II includes the scientific manuscripts originated from the research activity of this thesis and already accepted for publication in two scientific journals.

0.2.1 Summary of Publications

0.2.1.1 Scientific Journals

Paper A B. Sanchez, G. Vandersteen, R. Bragos and J. Schoukens, *Optimal Multisine Excitation Design for Broadband Electrical Impedance Spectroscopy*, Meas. Sci. Technol. 22 115601, 2011, doi:10.1088/0957-0233/22/11/115601, http://stacks.iop.org/0957-0233/22/115601

The aim of this work is to solve the problem of the optimal multisine excitation design for accurate Electrical Bioimpedance estimation. The *a priori* knowledge of the impedance spectrum enables to optimize the excitation in the frequency domain. As a result, the impedance spectrum accuracy is maximized for a discrete number of excited frequencies under energy and measuring time constraints. The main finding is the study of the contribution of the multisine amplitude power spectrum and frequency distributions to the Electrical Bio-Impedance accuracy for characterizing electrical impedance relaxations. Other findings of relevance are:

- The calculation of the EBI dispersion function and the study of its relation to the EBI accuracy.
- The influence of the multisine amplitude power spectrum and the number of excited frequencies and their distribution to the EBI accuracy.

Paper B B. Sanchez, J. Schoukens, R. Bragos and G. Vandersteen, *Novel Estimation of the Electrical Bioimpedance using the Local Polynomial Method. Application to in-vivo real-time Myocardium Tissue Impedance Characterization during the Cardiac Cycle*, Accepted for publication IEEE Transactions on Biomedical Engineering.

This paper presents a novel approach for impedance spectrum estimation, based on the Local Polynomial Method (LPM) for real-time time-varying Electrical Bio-Impedance (EBI) characterization. The LPM efficiently rejects the leakage error's influence on the impedance frequency response estimation when the EBI is under the effect of transients compared to the classical spectral analysis methods based on windows. The theory and instrumentation is supported by a set of validation measurements compared to a commercial impedance analyzer. The obtained results present relevant findings of a successful application of the LPM for real-time *in-vivo* myocardium tissue electrical impedance characterization. Further research should enable to detect how the systolic and diastolic function as well as cardyomiocyte contractile activity change during time in an ischemia process.

0.2.1.2 Conferences

- Sanchez, B., Vandersteen, G., Bragos, R. and Schoukens, J.: *A Novel Approach for Impedance Spectrum Estimation: the Local Polynomial Method.* International Workshop on Impedance Spectroscopy, Chemnitz, Germany. September 2011. Presented.

- Sanchez, B., Vandersteen, G., Rosell, J., Cinca, J and Bragos, R.: *In-cycle Myocardium Tissue Impedance monitoring using Impedance Spectroscopy based on Multisine excitation.* 33rd Annual International Conference of the IEEE Engineering in Medicine and Biology Society, Boston, USA. August 2011. Presented.

- Sanchez, B., Bragos, R. and Vandersteen, G.: *Influence of the multisine excitation amplitude design for biomedical applications using Impedance Spectroscopy.* 33rd Annual Internation Conference of the IEEE Engineering in Medicine and Biology Society, Boston, USA. August 2011. Poster.

- Llucia, A., Sanchez, B., Soler, C., Roura, S., Prat, C., Gálvez, C., Rosell, J., Bragos, R. and Bayes, A.: *Electrical stimulation for cardiac bioengineering with subcutaneous and cardiac adipose-tissue derived progenitor cells (ATDPCs).* European Society of Cardiology Congress. Paris, France. August 2011. Poster.

- Llucia, A., Sanchez, B., Soler, C., Roura, S., Prat, C., Gálvez, C., Bragos, R. and Bayes, A.: *Electrical stimulation of adipose tissue-derived progenitor cells (ATDPCs) of subcutaneous and cardiac origin for cardiac regeneration purposes.* Heart Failure Congress of the European Society of Cardiology. Gothemburg, Sweden. May 2011. Poster.

- Sanchez, B., Rosell, J. and Bragos, R.: *Multifrequency simultaneous bio impedance measurements using multitone burst for dynamic tissue characterization.* International Conference on Electrical Bioimpedance, Florida, USA. April 2010. Presented.

- Sanchez, B. and Bragos, R.: *Equipo compacto de medida de impedancia eléctrica multifrecuencia basado en señales multiseno.* XXVII Congreso Anual de la Sociedad Española de Ingeniería Biomédica CASEIB, Cadiz, Spain. November 2009. Presented.

- Sanchez, B. and Bragos, R.: *Fast Electrical Impedance Spectroscopy measurement techniques for dynamic bioimpedance characterization.* Barcelona

Forum on Ph.D. Research in Electronic Engineering, Barcelona, Spain. October 2009. ISBN 978-84-7653-398-7. Presented.

- Sanchez, B. and Bragos, R.: *Fast Electrical Impedance Spectroscopy for moving tissue characterization using Bilateral QuasiLogarithmic Multisine bursts signals.* 4th European Congress of the International Federation for Medical and Biological Engineering IFMBE. Antwerp, Belgium. November 2008. Presented.

- Sanchez, B., P.J. Riu i Costa, J. Rosell-Ferrer and Bragos, R.: *Espectroscopia de Impedancia Electrica para la caracterización de tejidos biológicos. Aplicación específica a medidas dinámicas.* XXVI Congreso Anual de la Sociedad Española de Ingeniería Biomedica CASEIB. ISBN 968-84-691-3641-6. Presented.

- Sanchez, B. and Bragos, R.: Fast EIS using a multisine burst for time varying biological system characterization. IBEC Symposium. Barcelona, Spain. November 2007. (Poster). Presented.

This page intentionally left blank.

Part I

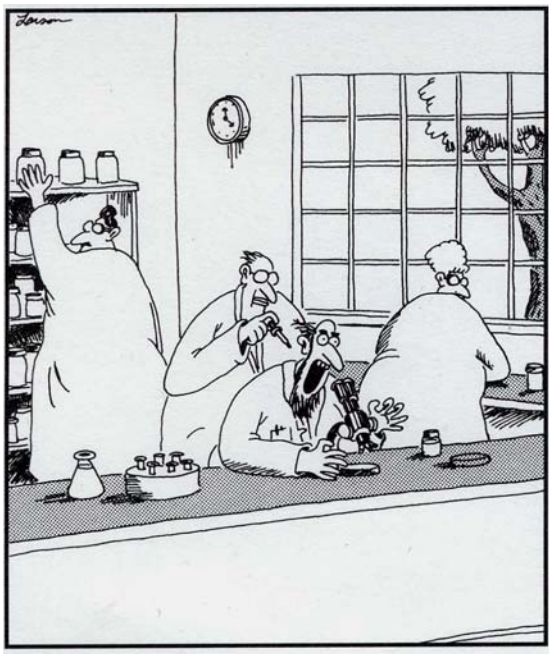

Professor Glickman, the lab practical joker, deftly places a single drop of hydrochloric acid on the back of Professor Bingham's neck.

The Far Side, by Gary Larson.

This page intentionally left blank.

Baldrick, no! It's the worst plan since Abraham Lincoln said "Oh I'm sick of kicking around the house tonight, let's go take in a show!".
.

-Blackadder (1983)

1

Introduction to Electrical Bio-Impedance (EBI)

Section 1.1 and 1.2 of Chapter 1 introduce the general concepts related to the study of dielectric properties of materials and their frequency response. The application to biological systems and living cells is referred as Electrical Bio-Impedance (EBI) and is described in Section 1.3. Finally, Sections 1.4 and 1.5 introduce the basics of Electrical Impedance Spectroscopy (EIS) and its main applications.

1.1 Basic Definitions

The Electrical Bio-Impedance (EBI) theory comes from the dielectric spectroscopy field, which measures the dielectric properties of a material as a function of frequency. It is based on the interaction between an external stimulus and the electric dipole moment of the biological sample, usually expressed as a function of its permittivity or conductivity. Furthermore, the cell membrane has a dielectric behavior that, in addition to the ionic conduction of the intra and extra cellular medium, constitutes the basic electrical phenomenon in the Electrical Impedance Spectroscopy (EIS) field when applied to biological materials.

A dielectric is an insulator material whose electrons are linked to the atoms that constitute it. Thus, the electrons can not move freely and will not generate conduction current. The effect of the electric field in these materials is a short movement in the charges with respect to the original position, known as polarization. Then, $\vec{D}$ is the electrical displacement vector and $\vec{J}$ the induced current defined as follows:

$$\vec{D} = \varepsilon_0 \vec{E} + \vec{P} \tag{1.1}$$

$$\vec{J} = \sigma \vec{E} \tag{1.2}$$

where $\vec{E}$ is the electric field vector, ε_0 is the vacuum's dielectric permittivity, σ is the conductivity and $\vec{P}$ the polarization vector. Taking into account that the polarization is caused by the electric field, it is possible to find the dependency between polarization and the electric field. Nevertheless, the electrical susceptibility of the material has to be known. In an anisotropic material, the polarization and the field have not necessarily the same direction. Then, each component of the polarization is related to the component of the electric field according to the polarization vector as follows (Malmivuo and Plonsey, 1995):

$$\vec{P}\left(\vec{r},t\right) = \varepsilon_0 \left(\mathrm{T}^{(e_1)} + \mathrm{T}^{(e_2)} + \mathrm{T}^{(e_3)} + \cdots\right) \cdot \vec{E}\left(\vec{r},t\right) \tag{1.3}$$

where $\mathrm{T}^{(e_i)}$ are in general tensors and correspond to the series Taylor's coefficients, also known as the electrical susceptibility of the material.

If an isotropic and homogeneous material is considered, which means that the polarization is independent from the field orientation and that the electrical properties of the material are independent of $\vec{r}$, the electrical susceptibility then becomes a scalar:

$$\vec{P}\left(\vec{r},t\right) = \varepsilon_0 e \vec{E}\left(\vec{r},t\right) \tag{1.4}$$

Therefore, the displacement vector defined in eq. 1.1 can be rewritten as:

$$\vec{D} = \varepsilon_0 \vec{E} + \varepsilon_0 e \vec{E} = \varepsilon_0 \left(1 + e\right) \vec{E} \tag{1.5}$$

Then, two parameters that characterize the material can be defined: the material's relative permittivity ε_r and the material's permittivity ε:

$$\varepsilon_r = \left(1 + e\right) \tag{1.6}$$

$$\varepsilon = \varepsilon_0 \varepsilon_r \tag{1.7}$$

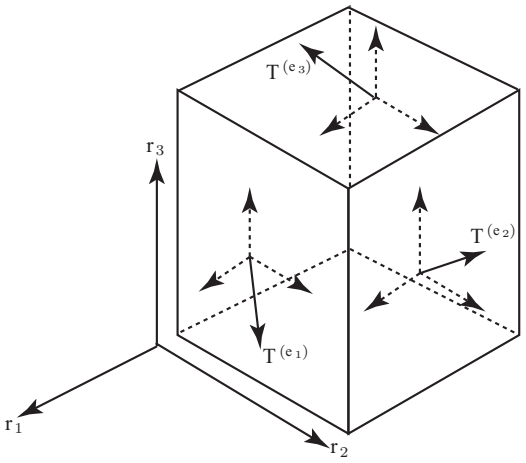

Figure 1.1: Electrical susceptibility tensor's components in a three-dimensional Cartesian coordinate system $\vec{r}$.

Finally, the displacement vector for any isotropic and homogeneous material results into:

$$\vec{D} = \varepsilon_0 \varepsilon_r \vec{E} \tag{1.8}$$

The same procedure can be followed for magnetic materials, so the magnetic intensity field can be written as follows:

$$\vec{B} = \mu_0 (1 + m) \vec{H} = \mu_0 \mu_r \vec{H} \tag{1.9}$$

where μ_0 is the vacuum permeability, m is the magnetic susceptibility factor, μ_r is the material's relative permeability and μ is the material's permeability.

1.1.1 Complex permittivity and conductivity

Until now, we have assumed that the electric and magnetic fields applied to the material did not suffer losses. This is a good approach in a vacuum environment. However, this is not necessarily true inside materials, neither in biological materials, where ionic currents are present in intra/extra cellular milieu. Considering the study in the sinusoidal steady state, permittivity and conductivity are complex numbers, denoted by the superscript $*$, usually defined as:

$$\varepsilon^* (\omega) = \varepsilon_i^{'} (\omega) - j \varepsilon_i^{''} (\omega) = \varepsilon_r - j \frac{\sigma}{\omega \varepsilon_0} \tag{1.10}$$

$$\sigma^* (\omega) = \sigma + j\omega\varepsilon_r\varepsilon_0 \tag{1.11}$$

and the relation between the complex conductivity and the permittivity is:

$$\sigma^* (\omega) = j\omega\varepsilon^* (\omega)\,\varepsilon_0 \tag{1.12}$$

Once the parameters that characterize materials are identified, that is σ, ε and μ, the next step is to define a section with known dimensions and the current distribution. A simple approach is to define a material volume formed by a cross-sectional area A separated by d length as is shown in Figure 1.2. As a

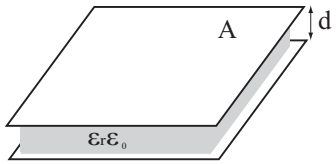

Figure 1.2: Two parallel conductive plates separated by a dielectric.

result, the equivalent capacitor created will present a capacity:

$$C = \varepsilon_r\varepsilon_0\frac{A}{d} \tag{1.13}$$

and a conductivity as follows:

$$G = \sigma\frac{A}{d} \tag{1.14}$$

So, the equivalent electrical impedance, which depends on the angular frequency ω, is related to the length d and the cross-sectional area A of the material according to:

$$Z (\omega) = \rho^* (\omega)\,\frac{d}{A} \tag{1.15}$$

where d/A is known as cell constant and has dimensions of $[m^{-1}]$. ρ^* is the complex resistivity and is expressed by:

$$\rho^* (\omega) = \frac{1}{\sigma^* (\omega)} = \frac{1}{\sigma + j\omega\varepsilon_r\varepsilon_0} \tag{1.16}$$

1.2 Dielectric relaxations

The dielectric response to an excitation is not instantaneous because time is needed to re-order the charges. In a first approximation, two assumptions are

made: (1) the material only has one relaxation process with a single characteristic time constant τ and (2) the polarization increases according to an exponential curve as a function of time. As a result, the dielectric response when applying an electric field step excitation can be considered as a first order response, which means that the response of dielectric to a sinusoidal excitation will depend on the frequency ω.

1.2.1 Frequency dependence of dielectric properties

The term dispersion is used to indicate that the observed electrical properties are related to dielectric losses associated with the relaxation of electric dipoles. Each of these dispersions are characterized by an average relaxation time τ. In the frequency domain, the dielectric expression is called the Debye's single dispersion equation:

$$\varepsilon^*(\omega) = \varepsilon_\infty + \frac{\varepsilon_s - \varepsilon_\infty}{1 + j\omega\tau} \tag{1.17}$$

where ε_s and ε_∞ are the complex values of permittivity in dc and high frequency respectively. Considering the effect of the static conductivity σ_s due to the free charges of the material, the following equation is obtained:

$$\varepsilon^*(\omega) = \varepsilon_\infty + \frac{\varepsilon_s - \varepsilon_\infty}{1 + j\omega\tau} - j\frac{\sigma_s}{\omega\varepsilon_0} \tag{1.18}$$

A similar procedure can be applied for the current density of the material:

$$\sigma^*(\omega) = \sigma_\infty + \frac{\sigma_s - \sigma_\infty}{1 + j\omega\tau} + j\omega\varepsilon_0\varepsilon_\infty \tag{1.19}$$

As mentioned above, both expressions are related. The modulus of the complex permittivity and conductivity are:

$$|\varepsilon(\omega)|^2 = \varepsilon_s \frac{1 + (\omega\tau_2)^2}{1 + (\omega\tau)^2} \tag{1.20}$$

$$|\sigma(\omega)|^2 = \sigma_s \frac{1 + (\omega\tau_1)^2}{1 + (\omega\tau)^2} \tag{1.21}$$

1.3 Electrical Bio-Impedance (EBI)

The term Electrical Bio-Impedance (EBI) refers to the opposition of a biological material to the pass of electrical current. Biological materials are formed

by millions of cells submerged into an ionic liquid. In essence, any cell can be simplified as a compartment with a watery interior that is separated from the external environment by a membrane (the plasma membrane) that prevents the free flow of molecules in and out of cells. In addition, each cell is internally formed by different organelles, i.e. nucleus, endoplasmatic reticulum, golgi apparatus and mitochondodria (see Figure 1.3 left). The basic function of the

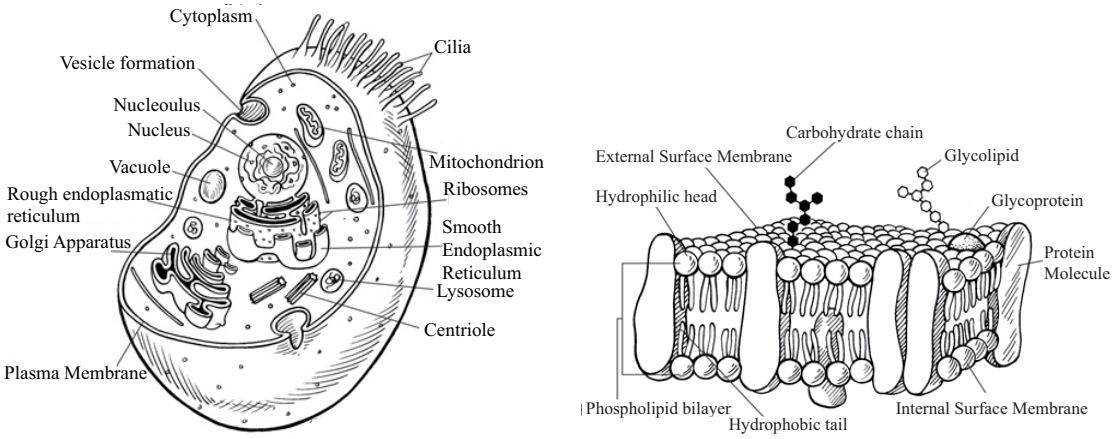

Figure 1.3: Schematic of a mammalian cell and some of its constituents (left); draft of the cell membrane's lipidic bilayer (right). Reproduced from (Alberts et al., 2002).

cell membrane is to control cell's communication. It is composed primarily of two layers of phospholipid molecules. The phospholipid have a "water-loving" (hydrophilic) end and a "water-hating" (hydrophobic) end. As it is shown in Figure 1.3 (right), the phospholipids are oriented with all the hydrophilic ends directed towards the inner and outer surfaces and the hydrophobic ends buried within the interior, forming a bilayer that acts like a barrier between the cell and the Extra Cellular Matrix (ECM). Moreover, the bilayer cell membrane contains cholesterol and protein channels that provide strength, flexibility and permeability characteristics.

In fact, the cell membrane presents an electrical impedance which is highly frequency dependent due to its high capacitive response. As is shown in Figure 1.4, low frequency currents mostly flow through the extra cellular liquid because the cell's membrane impedance is too big. Meanwhile, the high frequency currents flow through intra and extra cellular liquid. Then, the impedance will be bigger at low frequencies than in higher frequencies, giving as a result the relaxation of this impedance as a function of ω.

However, the structure of the biological material and its frequency's depen-

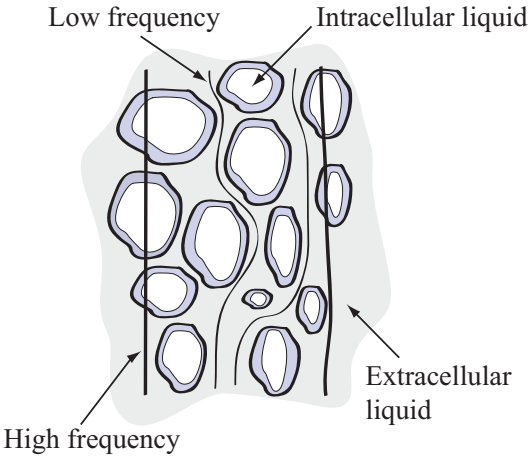

Figure 1.4: Alternating current flowing through a biological sample; low and high frequency density current lines flow through the Extracellular liquid and through the Extra/Intracellular liquid respectively.

dance is more complex than this simple approach. This is due to the fact that there are more factors involved. Therefore, the EBI information will be modified since a lot of cells exist in the tissue region of interest, and all of them contribute into the EBI measurement. Thus, the EBI provides useful information about the passive electrical properties of the tissue measured, which is directly related to its physiological state.

There are three main characteristic relaxations associated with the Electrical Bio-Impedance, each one related to a particular phenomenon. Figure 1.5 shows how the modulus of the permittivity and conductivity of the Electrical Bio-Impedance change with frequency:

- α is influenced by the intracellular structures, ionic dissemination and dielectric losses of the material. The frequency range is from mHz up to 10 kHz.

- β represents the interfacial polarization effects and it is the structural relaxation described in Figure 1.4. The frequency range is from 10 kHz up to 100 MHz and includes responses from intracellular structures.

- γ has information about the dipolar relaxations, i.e. water molecules and proteins. The frequency range is from 100 MHz up to 100 GHz.

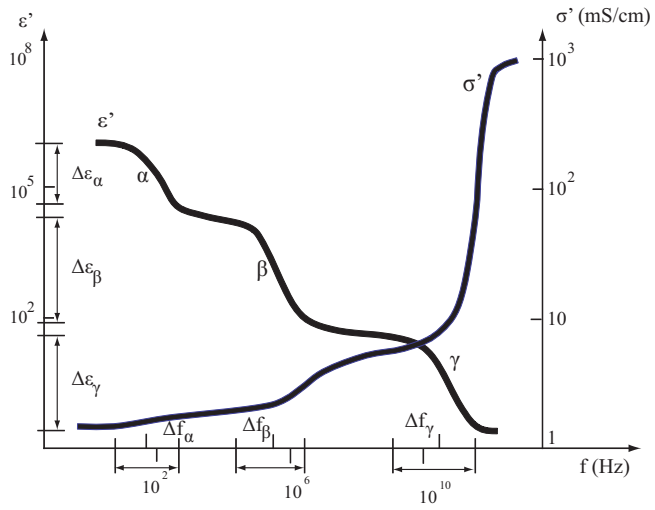

Figure 1.5: Dielectric permittivity ϵ (decreasing) and conductivity σ (increasing) as function of frequency. Reproduced from (Schwan, 1994).

1.4 Electrical Impedance Spectroscopy (EIS)

One of the techniques used for Electrical Bio-Impedance (EBI) measurements is the Electrical Impedance Spectroscopy (EIS). EIS has been widely used in clinical investigation, physiological research and medical diagnosis. In Section 1.5 there is a list of some examples of clinical applications.

In the field of biological materials and tissue engineering, EIS has contributed to the determination of the tissue and organs state. Historically, EIS measurements have been done using the classical sweep-sine technique. The measurement of impedance using this technique consists in applying an AC current to the biological system and then measuring the potential through the system. Supposing that we apply a sinusoidal current excitation $I(\omega)$ to a linear system, the response to this potential is an AC potential signal $V(\omega)$, containing the excitation frequency ω but with a different amplitude V and phase θ. The term impedance was introduced by Heaviside in 1886, when he considered both magnitudes as complex values. So, the impedance can be expressed as the ratio of the measured voltage response over the excitation current according to the Ohm's law:

$$Z(\omega) = \frac{V(\omega)}{I(\omega)} = \frac{V\cos(\omega t + \phi)}{I\cos(\omega t + \theta)} \tag{1.22}$$

Using Euler's relation, it is possible to express impedance as a complex number:

$$Z(\omega) = |Z| e^{j\varphi} = |Z| (\cos\varphi + j \sin\varphi) \tag{1.23}$$

where $|Z|$ is known as the impedance magnitude and φ the phase, defined by:

$$|Z| = \frac{V}{I} \qquad \varphi = \phi - \theta \tag{1.24}$$

1.4.1 Impedance representation

The magnitude and phase of a complex impedance $Z(\omega)$ value can be represented in a two-dimensional reference system. The phase of the imaginary number $e^{j\varphi}$ indicates the direction of the vector impedance magnitude $|Z|$. Complex impedance may be plotted in the plane with either rectangular or polar coordinates, as shown in Figure 1.6 where Z_{re} and Z_{im} are the real and imaginary part

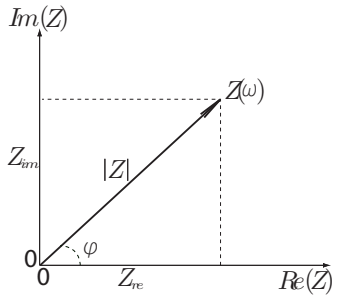

Figure 1.6: The impedance Z plotted as a vector on the complex plane.

of the complex impedance known in the literature as resistance and reactance respectively. Resistance and reactance are defined by:

$$Z_{re} = |Z| \cos(\varphi) \qquad Z_{im} = |Z| \sin(\varphi) \tag{1.25}$$

and they are also related to the magnitude and phase according to:

$$|Z| = \sqrt{Z_{re}^2 + Z_{im}^2} \qquad \varphi = \arctan \frac{Z_{im}}{Z_{re}} \tag{1.26}$$

1.4.2 Bio-Impedance electrical modeling

There are many different models of lumped parameters in order to electrically represent a biological system, from a single cell to more complex systems like

organs. A first approach for determining a simplified description of the macroscopic passive electrical properties of the tissue is to consider a model formed by a cellular suspension in an extracellular liquid. As shown in Figure 1.7, this assumption enables to model data within an electrical circuit given by three electrical components, usually described for representing the β relaxation: (1), R_e resistance models the impedance of the extracellular liquid, (2), R_i resistance models the intracellular liquid, and (3), C_m capacitor which models the membrane's capacitance.

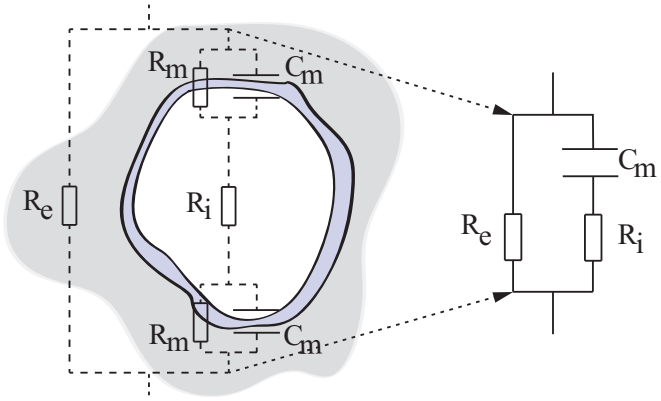

Figure 1.7: The equivalent circuit of a living cell including the R_m parameter, which models the membrane's resistance.

Due to the frequency behavior and its dependence on the cell's characteristics, it is possible to assign a frequency impedance relaxation for each type of tissue. Then, it is possible to identify different tissues located close to each other in the body (Rigaud et al., 1995). However, this simplified model is far from reality for many reasons. One reason is that it does not explain multiple relaxations. To overcome this limitation, in (Cole and Cole, 1941) was introduced the concept of distributed time constant for more accurate representations of the frequency response. This is modeled by the α parameter shown in eq. 1.18:

$$\varepsilon^* (\omega) = \varepsilon_\infty + \frac{\varepsilon_s - \varepsilon_\infty}{1 + (j\omega\tau)^{1-\alpha}} - j\frac{\sigma_s}{\omega\varepsilon_0} \tag{1.27}$$

where α is an empirical parameter characteristic of the distribution of the relaxation frequencies. When α is equal zero, the Cole-Cole equation is reduced to the Debye equation shown in eq. 1.18. It is possible to rewrite the Cole-Cole equation that models the complex permittivity shown in eq. 1.27 and considers

the electrical impedance as follows:

$$Z(f) = R_\infty + \frac{R_0 - R_\infty}{1 + \left(j\frac{f}{f_c}\right)^{1-\alpha}} \tag{1.28}$$

where the central frequency f_c is the frequency corresponding to the mean value of the distribution of the relaxation frequencies. As shown in Figure 1.8, the equation 1.28 represents an arc of circumference in the complex plane. The depression of the arc is defined by the α parameter. Impedance data plotted from Cole equation into the complex plane is usually referenced in the literature as Cole plot, although Nyquist, Bode or Wessel references are also used.

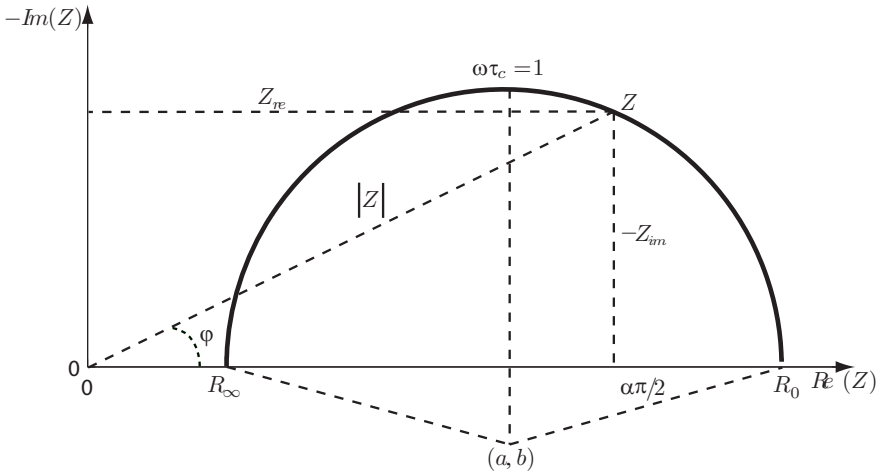

Figure 1.8: Representation of the complex plane of the impedance of the Cole plot.

A limitation that have the Cole equation (see eq. 1.28) and the Cole-Cole equation (see eq. 1.27) is that they do not explain overlapping relaxations. Despite of this, both are widely used for Electrical Bio-Impedance analysis. However, an alternative to the distributed time constant was proposed in (McAdams and Jossinet, 1995) when multiple relaxations are present. It is based on modeling a pseudocapacitor with constant phase element. Another possibility is to associate different serial R_iC_i branches where each branch models a specific relaxation. All the mentioned branches are in parallel with an unique resistance that models the extracellular liquid. A discussion of the convenience of connecting equivalent electrical components in series or in parallel is available in (Smith, 1995).

1.5 Electrical Bio-Impedance applications

Electrical Impedance Spectroscopy (EIS) is a widespread technology that, during the past few years, has become increasingly popular. Proof of this success is that there are numerous applications that have evolved not only in clinical investigations, physiological research and medical diagnosis and imaging but also for food processing (Pliquett, 2010), electrochemical (Orazem and Tribollet, 2008) and biotechnological fields. There are many examples of medical applications, e.g body composition determination (Kyle et al., 2004), skin cancer detection (Aberg et al., 2004), and Electrical Impedance Tomography (EIT) (Brown, 2003) among others. Through animal *in-vivo* and *ex-vivo* experimentation, tissue electrical impedance has been shown to correlate with many physiological states of the tissue (Valentinuzzi et al., 1996), e.g. the regional and global ischemia processes in myocardium (Salazar et al., 2004), edema (Schaefer et al., 2002), and detection of rejection episodes following heart transplantation (Grauhan et al., 1996; Cinca et al., 1998). In electrochemical field, EIS has been widely used as a detection tool for many different types of biosensors (Bao et al., 2008; Lisdat and Schäfer, 2008) and to study complex reaction mechanisms, corrosion reactions, surface changes, and properties of semiconductor materials.

Most of the previously cited EIS applications are based on frequency impedance measurements using frequency sweep technique. A classical example is the characterization of the myocardium tissue state using electrical impedance. This is usually performed at a single frequency, in the 1 kHz - 10 kHz range (Fallert et al., 1993) or performing a frequency sweep from 1 kHz to 1 MHz (Gersing, 1998; Salazar et al., 2004). Both *in-vivo* single-frequency and multifrequency studies have been reported in (Fallert et al., 1993) for the ischemic tissue (Mellert et al., 2010) and healed scar (Cinca et al., 1998). Although the time variation of the impedance signal has information about the tissue dynamics, this information has been usually underestimated in all those single-frequency or frequency-sweep EIS experiments. This is due to the fact that, on one hand, measuring in a single excited frequency just contains information of the impedance spectrum at this excited frequency. On the other hand, the sweep technique has a measuring time which can be much longer than the system dynamics. As a consequence of this, the measurements are corrupted by noise because the system non-stationary behavior is undersampled. This noise can be reduced by averaging successive frequency sweeps measurements. Thus, yielding an excessively long measuring time for a clinical diagnostic tool and losing the non-stationary information. In the end, any of the measurements have information about the

mentioned dynamics.

A different Electrical Impedance Spectroscopy approach based on broad-band excitations enables to collect multiple impedance spectrum data within a reduced measuring time. Practical examples which would profit of this technique would not only be biomedical applications for cardiovascular or respiratory systems characterization, but also the understanding of various unsolved problems in a wide range of applications where the system non-stationary behavior is of interest.

This page intentionally left blank.

Igor: Dr. Frankenstein...
Dr. Frederick Frankenstein: "Fronkensteen."
Igor: You're putting me on.
Dr. Frederick Frankenstein: No, it's pronounced "Fronkensteen."
Igor: Do you also say "Froaderick"?
Dr. Frederick Frankenstein: No... "Frederick."
Igor: Well, why isn't it "Froaderick Fronkensteen"?
Dr. Frederick Frankenstein: It isn't; it's "Frederick Fronkensteen."
Igor: I see.
Dr. Frederick Frankenstein: You must be Igor. [*He pronounces it ee-gor*]
Igor: No, it's pronounced "eye-gor."
Dr. Frederick Frankenstein: But they told me it was "ee-gor."
Igor: Well, they were wrong then, weren't they? .

-Young Frankstein (1974)

2

Broadband Electrical Impedance Spectroscopy (EIS)

This chapter covers the problem of measuring biological systems, which is under the discussion of this thesis, by means of Electrical Impedance Spectroscopy using broadband excitations. A first introduction to the simultaneous multifrequency Electrical Bio-Impedance (EBI) measurements is described in Section 2.1. Following, Section 2.2 introduces the motivation of measuring using broadband excitations. Next, Section 2.3 presents the time - frequency properties of the most common broadband excitations, including a short description of their advantages and disadvantages. Section 2.4 and 2.5 show the influence of the excitation choice on the impedance spectrum accuracy. In Section 2.6 broadband excitations that allow short time EIS are reviewed and compared according to the impedance spectrum accuracy.

2.1 Introduction

Electrical Impedance Spectroscopy (EIS) can be used to characterize biological materials in a wide variety of applications as described in Section 1.5. Classic

EIS based on frequency sweep needs averaging to remove the time modulations induced by the electrical and mechanical properties of the biological systems which are time-varying. The potentially useful information contained in the modulation is lost unless a synchronous averaging technique is used. In contrast to classical EIS, broadband signals overcome this limitation and enable multiple EBI spectrum data collection in a reduced measuring time. Nevertheless, the price to pay resides in the intrinsic loss on the impedance spectrum accuracy. However, such loss of accuracy can be minimized by an appropriate choice of the excitation as well as its time and frequency properties. This means that the excitation can be optimized for maximizing the information from the measurements. That is, to obtain the most accurate EBI spectrum.

2.1.1 Historical overview

There are many different types of electrical stimuli which are used in EIS. The most common among the various approaches to EIS experiments is the application of a single frequency sinusoidal current stimulus to the system under test. Then, the phase shift and amplitude of the resultant voltage of the response are measured. The impedance spectrum can be determined by sweeping the exciting frequency in the frequency range of interest. The major advantage of this approach relies on the fact that a high Signal-to-Noise Ratio (SNR) is obtained while increasing the measuring time. For many Electrochemical applications, this method has been widely used. It is based on a single-sine ac wave of a given frequency which is overlaid on a dc bias potential and then applied to the working electrode. This process is repeated by scanning the frequency and computing the impedances from the ac voltage and current data at desired frequencies. Problems with this approach arise primarily from the relatively long data-acquisition time required for acquiring the whole impedance spectrum. This is the reason why the frequency sweep technique is discarded in those applications where high throughput real-time data and on-line monitoring are required. This method is viable only for a stable and reversible system in equilibrium, as the system's linearity, stability, and causality must be ensured (Hubin et al., 2005). However, because of the fact that biological objects are highly sensitive to the electric field applied (Pliquett, 2004; Pliquett and Schoenbach, 2009), this transformation is only valid when the signal makes the system steady state response to be linear. This means that excitations are peak limited to ensure a linear response of the system under test. When talking about biological measurements, safety restrictions regarding the energy applied should be considered aside from the peak amplitude limitation for linearity considera-

tions. A practical example where energy and measurement time are limited is in *in-vivo* patient clinical procedures, where the norm IEC/UL 60601-1 specifies that the total current injected can not exceed 10 mA *rms* in any case.

In efforts to reduce the measurement time, researchers have proposed methods without frequency scanning. Measurements of full impedance spectra were not made until the 1970s, with publications reported in (Creason and Smith, 1972; Schwall et al., 1977). Their approach was based on the application of a mixed ac waves of many different frequencies superimposed on a desired dc bias potential to an electrochemical system. The resultant current signal was deconvoluted into the component frequencies employing the Fast Fourier Transform (FFT). The impedance was then calculated at each frequency using the original ac voltage, and the ac current was obtained from the deconvolution of the current signal. During the same time, a Maximum Length Binary Sequence (MLBS) generator based on a shift register for characterizing RC circuits was presented in (Ichise et al., 1974). Later on, the same excitation was applied to determine the state of bone fractures (Schneider, 1996). Different broadband impedance analyzer systems have been reported since then in (Hartov et al., 2000; Morgan et al., 2007; Nacke et al., 2007). Apart from the previously mentioned excitations, there are other signals which have already been described in (Min et al., 2010, 2004) and applied to different biomedical applications (Bragos et al., 2001; Ogunnika et al., 2008). More recent examples of applications can be found in (Sun et al., 2007b; Cheung et al., 2010) for single cell characterization using microfluidic devices.

2.2 Broadband EIS measurements

In contrast to the frequency sweep approach, broadband EIS offers the advantage of simultaneous frequency response data collection. This is due to the fact that broadband excitation spreads the energy at several frequencies at the same time, which is reflected into a short measuring time. However, the weakness of such kind of fast EIS measuring techniques is its intrinsic loss of accuracy. In the end, the total measuring time does not only depend on the impedance spectrum accuracy desired, but also to the broadband signal applied, its time/frequency features, the system non-stationary properties and the signal processing techniques used.

Because there are many broadband excitations, each one with its own time and frequency properties, a signal quality metric is needed to compare between them. For instance, a metric to measure how much amplitude is consumed by

the signal to inject a certain power level into the system is needed in order to be able to compare the time and frequency properties. Although there are many merit figures proposed in the literature (Godfrey et al., 1999), the most popular by far is the Crest Factor (CF). This is because its interpretation is simple, even by visual inspection.

2.2.1 Crest Factor

Before defining the Crest Factor it is convenient to define the norm of the function $u(t)$, denoted by $l_p(u)$ (Guillaume et al., 1991), taken over the interval where the excitation is defined [0,T] as:

$$l_p(u) = \left[\frac{1}{T} \int_0^T |u(t)|^p \, dt \right]^{1/p}, p \geq 1 \tag{2.1}$$

The Chebyshev norm l_∞ (also known in the literature as the minimax norm, the uniform norm or the maximum norm) of a continuos function $u(t)$ is defined as its peak value in the interval [0,T]:

$$l_\infty = \max_{t \in [0,T]} |u(t)| \tag{2.2}$$

Finally, the Crest Factor of a function $u(t)$ is then defined as the ratio of its peak value and its root mean square value (RMS):

$$CF(u) = \frac{l_\infty(u)}{l_2(u)} \tag{2.3}$$

Another interpretation of the Crest Factor is possible using the Parseval's theorem:

$$CF(u) = \frac{l_\infty}{\sqrt{\sum_{\forall \omega \in \Omega} U(\omega) U^*(\omega)}} \tag{2.4}$$

where $U(\omega)$ is the excitation power spectrum. Note that the Crest Factor is defined in the frequency band Ω where the impedance spectrum is going to be measured. This means that the injected power described by the denominator term is limited to the excited frequencies being measured. In other words, any power that is injected outside this band will contribute to excite the system, but it will not contribute to obtain more information from the measurements.

To sum up, the Crest Factor gives an idea of the signal's compactness measuring how well distributed the signal values are over the excitation amplitude range. A small Crest Factor means that most of the amplitude elements in the excitation are distributed close to the minimum and maximum values of the signal. In contrast, a large Crest Factor means just the opposite: the amplitude elements are spread in a poor amplitude range. For a certain amplitude level, the lower the Crest Factor, the better because more measurement power is provided to the system. The relation between the Crest Factor and the Signal-to-Noise Ratio (SNR) from a linear time invariant system measurement is described in Section 2.2.1.1. The possible values for Crest Factor range from 1 up to ∞, with the limits representing the best and worst possible cases. Crest Factor reduction allows, on one hand, a larger energy to be injected for a given input range of the measurement device, avoiding then to run into A/D or D/A saturations. On the other hand, small CF keeps the system working in the linear region. This is is extremely important when exciting biological systems in order to prevent tissue stimulation.

2.2.1.1 Influence of the Crest Factor on the Signal-to-Noise Ratio (SNR)

The SNR of an ideal b-bit A/D converter measured over the Nyquist bandwidth (dc - Fs/2) without considering distortions when measuring a multisine input signal is decreased due to the Crest Factor and the number of exciting frequencies N as follows:

$$SNR = 6.02b + 1.76 - 20\log_{10}\left(\frac{CF}{\sqrt{2}}\right) - 10\log_{10}N \tag{2.5}$$

Hence, the Effective Number of Bits (ENOB) is given by

$$ENOB = \frac{SNR - 1.76 + 20\log_{10}\left(\frac{CF}{\sqrt{2}}\right) + 10\log_{10}N}{6.02} \tag{2.6}$$

which means that given a Signal-to-Noise Ratio (SNR), the smaller Crest Factor multisine excitation the better because less bits are needed to obtain the specified accuracy from the measurement.

2.2.2 Impedance Spectrum accuracy

Consider the impedance spectrum Z_k^0 as the mean impedance spectrum magnitude determined from M averages at exciting frequency k by applying the

classical spectral analysis based on cross and auto power spectrum using a rectangular window. The impedance spectrum variance σ_Z^2 is calculated from the input-output current and voltage noise estimation σ_I^2 and σ_V^2 (Schoukens et al., 2009b) as follows:

$$\begin{aligned} Z_k^0 &= \tfrac{1}{M} \sum_{n=1}^{M} Z_k^n \\ \sigma_{Z_k}^2 &= \tfrac{|Z_k^0|^2}{M} \left(\tfrac{\sigma_{I_k}^2}{|I_k^0|^2} + \tfrac{\sigma_{V_k}^2}{|V_k^0|^2} - 2\Re e \left(\tfrac{\sigma_{V_k I_k}^2}{I_k^0 \overline{V_k^0}} \right) \right) \end{aligned} \tag{2.7}$$

where I_0, σ_I^2 and V_0, σ_V^2 correspond to the mean spectrum magnitude and the variance of Fourier transformed current and voltage coefficients respectively, given by:

$$\begin{aligned} I_k^0 &= \frac{1}{M} \sum_{n=1}^{M} I_k^n \\ \sigma_{I_k}^2 &= \frac{1}{M(M-1)} \sum_{n=1}^{M} \left(I_k^n - I_k^0 \right)^2 \\ V_k^0 &= \frac{1}{M} \sum_{n=1}^{M} V_k^n \\ \sigma_{V_k}^2 &= \frac{1}{M(M-1)} \sum_{n=1}^{M} \left(V_k^n - V_k^0 \right)^2 \\ \sigma_{V_k I_k}^2 &= \frac{1}{M(M-1)} \sum_{n=1}^{M} \left(V_k^n - V_k^0 \right) \overline{\left(I_k^n - I_k^0 \right)} \end{aligned} \tag{2.8}$$

Note that from the previous expression it is possible to calculate the impedance spectrum Signal-to-Noise Ratio (SNR), defined at the excited line k as follows:

$$SNR_{Z_k} = \frac{\left| Z_k^0 \right|^2}{\sigma_{Z_k}^2} \tag{2.9}$$

Given the general expression of the variance of the impedance spectrum measurement (see eq. 2.7), it can be shown that the impedance spectrum SNR can be approximated by:

$$\frac{1}{SNR_Z} \approx \frac{1}{SNR_I} + \frac{1}{SNR_V} \tag{2.10}$$

The Noise-to-Signal Ratio (NSR) is, by definition, the inverse of the SNR. Then, the previous equation can be rewritten as:

$$NSR_Z \approx NSR_I + NSR_V \tag{2.11}$$

Then, the SNR on both current and voltage measurements should be maximized if accurate impedance spectra are desired. At this point, the aim of studying the time / frequency features of signals and its influence on the impedance spectrum accuracy at the exciting frequencies within the experiment constraints becomes more important. This is discussed in Section 2.3.

2.3 Strengths and weaknesses of periodic broadband signals for impedance spectroscopy

This section compares some general properties of spread-spectrum periodic signals for frequency response function measurements (Pintelon et al., 1997; Godfrey et al., 1999; Schoukens et al., 2000). The studied excitations are chirp (Min et al., 2007, 2008, 2010; Paavle et al., 2010), Maximum Length Binary Sequences (Godfrey, 1991; Rees et al., 1992; Tan and Godfrey, 2002; Godfrey et al., 2005), Discrete Interval Binary Sequences (van den Bos and Krol, 1979) and multisine signals (Schroeder, 1970; Van Der Ouderaa et al., 1988; Schoukens et al., 1991; Guillaume et al., 1991; Horner and Beauchamp, 1996; Simon and Schoukens, 2000; Vanhoenacker et al., 2001).

2.3.1 Maximum Length Binary Sequences (MLBS)

The Maximum Length Binary Sequences (MLBS) are binary periodic signals generated digitally. They can be easily implemented with very few hardware resources using a Linear Feedback Shift Register (LFSR) (see Figure 2.1). From all the possible Pseudo-Random Binary Sequences (PRBS) that can be generated with a fixed register length, the Maximum Length Binary Sequences (MLBS) are these PRBS sequences with the longest period and the shortest autocorrelation length, which is an approximation of a Dirac pulse. In practice, MLBS are based on a cascade of D flip-flops using the appropriate XOR feedback function in order to obtain the longest period. The LFSR is a shift register which, using feedback, causes the value in the shift register to cycle through a set of unique values. For a given clock frequency and register length n, and for all the possible initial non-zero values of the LFSR, the length of the MLBS is:

$$L = 2^n - 1 \tag{2.12}$$

LFSR feedback can be implemented in two ways: using the Fibonacci or the Galois form. When implemented in hardware, the Galois topology is usually

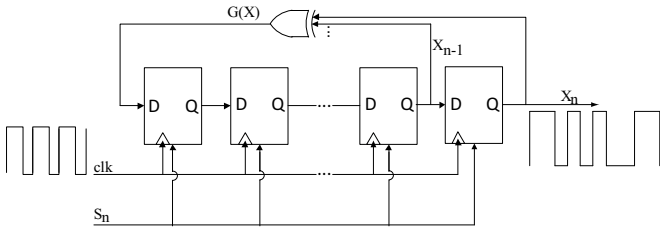

Figure 2.1: Fibonacci LFSR topology. The outputs of some registers are XORed with each other and the result $G(x)$ is fed back to the input of the shift register; s_n is any initial sequence of values except all zeros.

preferred due to its reduced number of logic gates in the feedback function. MLBS are very popular due to its implementation simplicity and its autocorrelation properties. As shown in Figure 2.2 (bottom), the MLBS amplitude power spectrum is relatively flat. This behavior is due to the *sinc* introduced by the zero-order hold at the output. However, a MLBS has an amplitude spec-

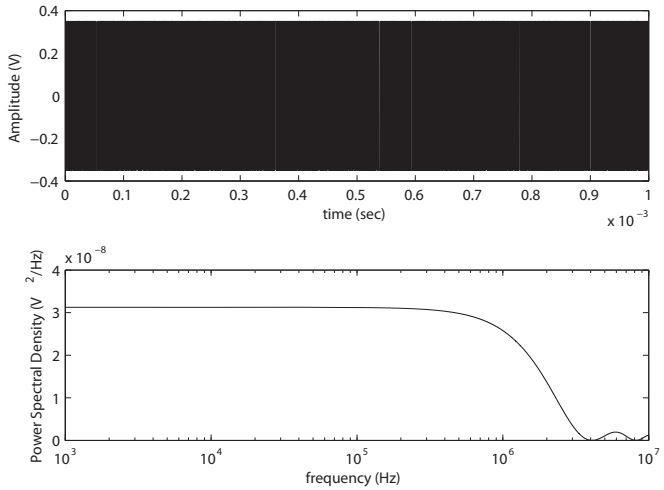

Figure 2.2: MLBS in time (top) and power spectral density (bottom).

trum whose components decrease inversely proportional to the frequency. This means that its resulting SNR will be lower compared to a single or a set of frequencies because the energy is distributed over the whole frequency range. The MLBS signals are binary, so they have the strength that it are robust to noisy environments and they also have the optimal full-band Crest Factor. Nevertheless, MLBS signals are highly sensitive to crosstalk and non-linear behaviors. As shown in (Schoukens et al., 1988), the MLBS CF varies as a function of

the spectral band in use (see eq. 2.4), decreasing towards 1 as the band increases towards infinity. In other words, not all the MLBS power is focused on the frequency band of interest, and part of it is wasted in exciting unwanted frequencies.

2.3.2 Discrete Interval Binary Sequences (DIBS)

The Discrete Interval Binary Sequences (DIBS) are periodic binary multifrequency sequences (see Figure 2.3 top), in which the sign of the signal can change only at an equidistant discrete set of points during time (van den Bos, 1967; van den Bos and Krol, 1979). As a result of this, a great part of the excitation power is concentrated in the desired frequency subband. In contrast to the sweept sine and the MLBS excitations, the DIBS amplitude power spectrum (see Figure 2.3 bottom) can be optimized by choosing the appropriate switching sign sequence. Since the DIBS excitations are binary, their full-band Crest Factor is 1. The author does not have any reference about applying DIBS for multifrequency EIS analysis despite their inherent superior properties to the MLBS. In contrast to the MLBS sequence, DIBS focus most of the excitation

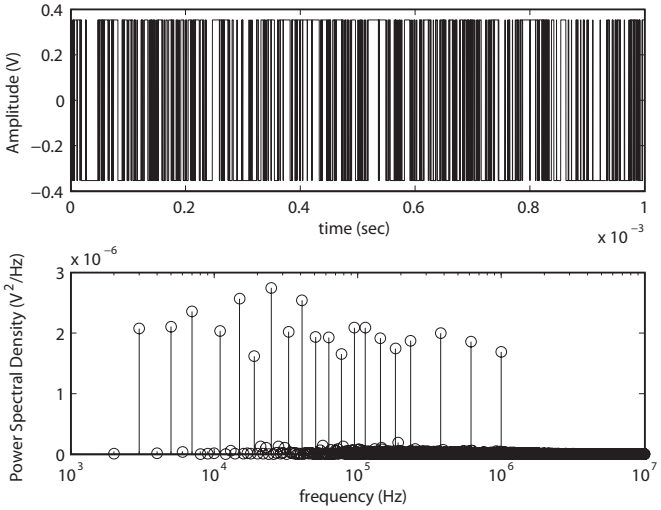

Figure 2.3: DIBS in time (top) and power spectral density (bottom).

energy at a user-defined set of interesting frequencies. In this case, the energy at the exciting frequencies represent about the 86 % of the overall excitation energy.

2.3.3 Chirp

The Chirp excitation is a sine sweep excitation that can easily be implemented using a Direct Digital Synthesizer (DDS) or using an Arbitrary Waveform Generator (AWG) defining the excitation parameters set. The corresponding time domain function for a linear chirp is given by:

$$u(t) = A\sin\left((at+b)\cdot t\right) \quad 0 \le t < T \tag{2.13}$$

where T is the sweep period, $a = \pi\left(f_{\max} - f_{\min}\right)/T$ is known as chirp rate, $b = \pi f_{\min}$. f_{min} and f_{max} represent the lowest and the highest frequency respectively. There are many chirp excitations depending on the frequency variation with time. Chirp excitations with a frequency variation which is swept up or down are known as up-chirp or down-chirp respectively. Compared to a multisine excitation, a chirp excitation is easily generated and all its extreme amplitude values are the same. As a result, Chirp excitations have a low Crest Factor (typically about 1.45). However, the main drawback is the lack of freedom in choosing an arbitrary amplitude power spectrum. As shown in Figure 2.4 (bottom), the chirp amplitude power spectrum is neither really flat at low frequencies, nor in the wanted frequency band, due to the ripple.

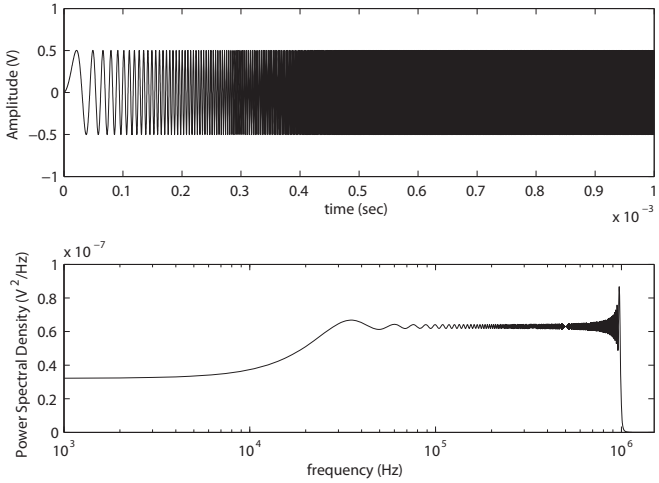

Figure 2.4: Up-Chirp in time (top) and power spectral density (bottom).

2.3.4 Multisine

The application of multisine excitations for frequency domain analysis has been widely described in (Schoukens and Pintelon, 1990; Schoukens et al., 1991; Schoukens and Dobrowiecki, 1998; Schoukens et al., 2000; Simon and Schoukens, 2000; Rolain et al., 2006). The idea behind the multisine signal is to keep the advantages of the sine wave, but to reduce the measurement time. To this end, the multisine signal expression is formed by the sum of N frequencies, each one with its own amplitude and phase. The time signal expression for a real-valued multisine signal can then be represented by a Fourier series, i.e., a trigonometric sum of order N:

$$u(t) = \sum_{n=1}^{N} a_n \cos(2\pi f_n t + \varphi_n) \tag{2.14}$$

where N is the number of exciting frequencies, a_n are the fundamental amplitudes and φ_n the phases. If no specific prior knowledge of the system is available, the amplitudes are often designed to be equal to excite the system with a flat amplitude spectrum. If the frequency response function is more or less known in advance, a_n can be tuned to decrease the uncertainty of the estimated transfer function (see Paper A for more information about how to design and optimize a multisine signal).

2.3.4.1 Multisine time properties

The resulting Crest Factor for a real multisine using Parseval theorem is given by:

$$CF = \sqrt{2}\frac{\|u\|_\infty}{\|a\|_2} \tag{2.15}$$

with a vector a containing the sinewave amplitudes a_n (see Appendix). Phases φ_n have to be chosen carefully because they influence the time-domain signal shape. Notice that while the multisine rms level is independent of the phase angles, its peak value is strongly dependent on them. For a given constant sequence of Fourier's coefficient a_n, the minimization of Crest Factor with respect to the multisine phases relies on finding the optimal phases that minimizes the Chebychev norm of the signal.

If all sine (or cosine) waves are set to a 0 degrees phase relation, the peaks will add coherently producing a maximum peak amplitude equal to the sum of the individual sinewave peak amplitudes. To illustrate this, Figure 2.5 shows the resulting multisine, where the Crest Factor is proportional to the square root of N. This will be the maximum possible Crest Factor for the particular

excitation power spectrum. Hence, the worst Crest Factor for a real multisine of unity amplitude tones is $\sqrt{2N}$, which means that the worst-case multisine periodic overshoot is $u_{rms}\sqrt{2N}$.

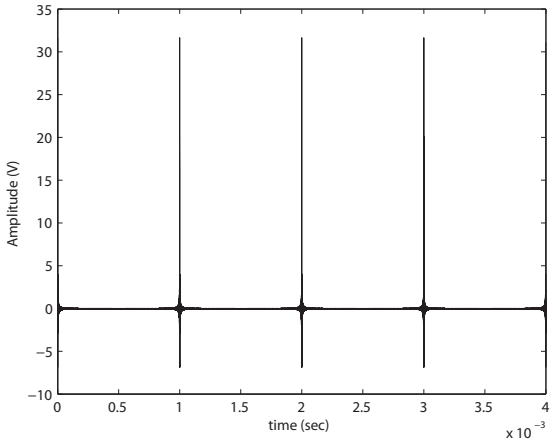

Figure 2.5: Flat multisine in time using 0 degree phases (CF=44.72).

The way to control the Crest Factor is to choose the phases of the multisine appropriately. Minimizing the multisine Crest Factor is not a straightforward task since the l_∞ norm is non-differentiable. This problem was already treated in (Beller and Newman, 1971), who proposed:

$$\varphi_n = \frac{\pi n^2}{N}, \quad n = 0, ..., N-1 \tag{2.16}$$

to minimize the multisine Crest Factor. Figure 2.6 shows how good it works if unity amplitudes $a_n = a^* > 0, \quad n = 0, ..., N-1$, are chosen. Note that Newman phases only need the number of N exciting frequencies as *a priori* information. An alternative approach was proposed in (Schroeder, 1970). The only assumption is that the number of exciting frequencies in the specified power spectrum is large and they are concentrated in a bandwidth that is small compared to its center frequency:

$$\varphi_m = \varphi_0 - 2\pi \sum_{n=0}^{m-1} (m-n) \cdot \frac{|a_m|^2}{\sum_{k=0}^{M-1} |a_k|^2}, \quad m = 1, ..., M-1, \quad \varphi_0 \in [-\pi, \pi] \tag{2.17}$$

In contrast to the Newman phases, the Schroeder phases (see Figure 2.7) take the amplitudes into account and therefore often gets better results in the case

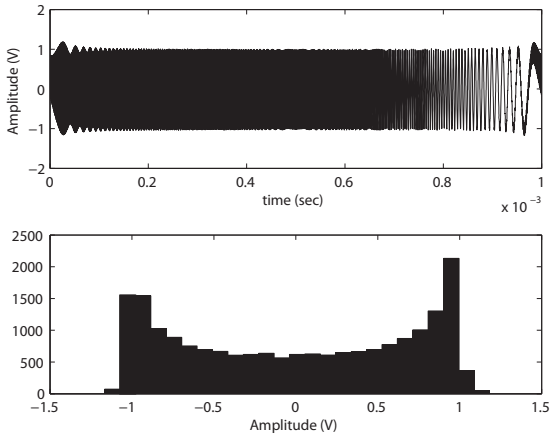

Figure 2.6: Flat multisine using Newman phases (top) and its amplitude histogram (bottom) (CF=1.67).

of non unity amplitudes. In the case of unity amplitudes the Schroeder phases simplifies to:

$$\varphi_m = \varphi_0 - \frac{2\pi}{M}\sum_{n=0}^{m-1}(m-n) = \varphi_0 - \frac{2\pi}{M}\cdot m\cdot(m+1), \quad m = 1,...,M-1, \quad \varphi_0 \in [-\pi,\pi] \tag{2.18}$$

which for $\varphi_0 = 0$ corresponds to the negative Newman phases (see eq. 2.16) and an additional linear term. The additional linear term is irrelevant, be-

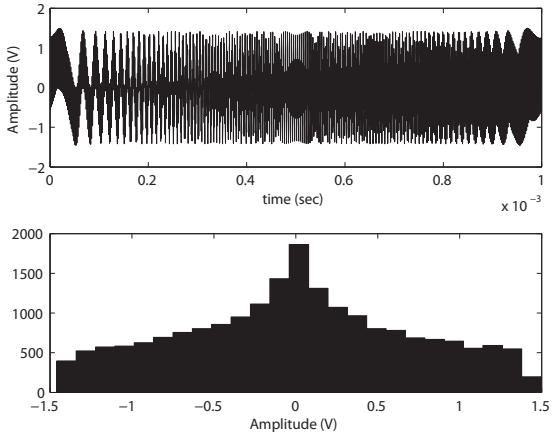

Figure 2.7: Flat multisine in time using Schroeder phases (top) and its amplitude histogram (bottom) (CF=2.12).

cause it corresponds simply to a shift in the starting time of the multisine. Schroeder's phases give reasonable results when the user-defined spectrum is flat and wideband, but under other conditions (i.e. bandlimited or in the presence of harmonic suppression), the results can be very undesirable (Pumplin, 1985).

Another option is to design the multisine excitations based on uniformly distributed random phases between 0 and 2π.

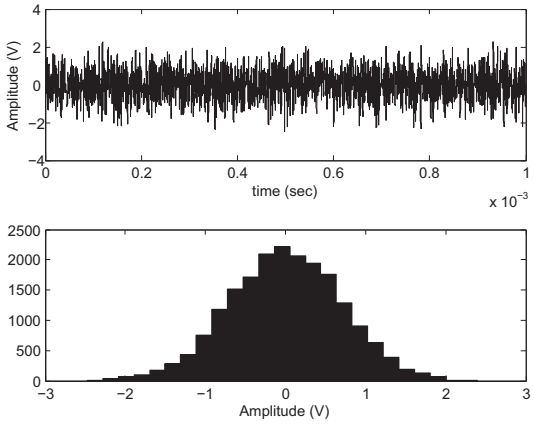

Figure 2.8: Flat multisine in time using random phases (top) and its amplitude histogram (bottom) (CF=3.10).

As shown in Figure 2.8, the random phases make the multisine amplitude Probability Density Function (pdf) to be almost Gaussian distributed with zero mean. In time domain, the random multisine looks like white noise, and that is the reason why they are known as periodic noise. In contrast to the pure periodic random noise, the amplitudes of a random multisine are not random.

If the goal is to design the multisine phases for characterizing a system with maximal SNR, then the random multisine is not the best solution. The best option is to design multisine phases such that the multisine amplitude pdf signal has almost a binary behavior (see Figure 2.9). In this case, almost all the multisine energy is focused on the maximum excitation amplitude. This is the same as minimizing the multisine Crest Factor, where the phases compress the excitation maximum peak. Related solutions to system identification and parameter estimation of linear systems were shown in (Van Der Ouderaa et al., 1988). Classical approaches use heuristics or analytical methods to arrange phase angles (Guillaume et al., 1991). Latest approaches use some kind of algorithm to improve results, i.e. Genetic Algorithms (GA) or solving the optimization

problem with a Non-Linear Solver (NLS) (Horner and Beauchamp, 1996; Mittelmann et al., 2006; Lee et al., 2003). However, the optimization problem of minimizing the Crest Factor of a multisine signal under time domain constraints represents a challenging computational task: it is always nonlinear, either in the objective function, in the constraints or in both. In addition, it is non-smooth as a consequence of the Chebyshev norm in the objective function. Hence, it can take a very long time to solve the highly nonlinear equality constraints.

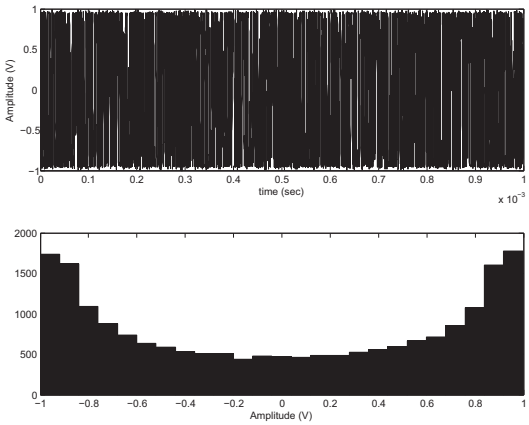

Figure 2.9: Flat multisine in time with numerically optimized phases (top) and its amplitude histogram (bottom) (CF=1.45).

2.3.4.2 Multisine frequency properties

From the frequency domain point of view, the multisine spectrum is obtained computing the Fourier Transform of eq. 2.14:

$$S_u(\omega) = 2\pi \sum_{n=1}^{N-1} \frac{a_n^2}{4} \left[\delta(\omega - \omega_n) + \delta(\omega + \omega_n)\right] \tag{2.19}$$

where a_n and ω_n can be designed to place the signal power very precisely to the exciting frequencies. The multisine frequencies ω_n are typically distributed logarithmically or equally-spaced. From the point of view of measuring Electrical Bio-Impedance, both present great disadvantages.

Equidistant frequency distribution has two inconveniences: (1) a high number of exciting frequencies are needed to cover the EIS frequency range to avoid loosing impedance spectrum resolution, and (2) any real system is inherently non-linear. As shown in (Vanhoenacker et al., 2001), the harmonic frequencies

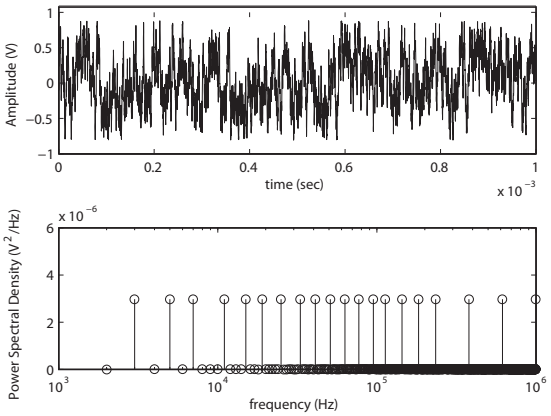

Figure 2.10: Multisine time (top) and its power spectral density (bottom) (CF=2.30).

introduced by even nonlinearities will be placed at the same even frequencies being excited, resulting into a mislead on the estimation of the impedance spectrum amplitude.

Pure logarithmic frequency distribution also has drawbacks: (1) there is a great number of exciting frequencies at low and high frequencies, which do not contribute to characterize the impedance relaxation, and (2) the vast majority of the low-cost electronic devices used present limitations at very low or very high frequencies.

One approach to overcome harmonics effect consists on generating each exciting frequency as a result of a fundamental frequency multiplied by a special sequence value. This solution is based on special sets of multipliers K_n that are chosen in order to accomplish as many as possible disjunct distortion signal frequencies and fundamentals signal frequencies. If the multipliers are only odd integers, the even order harmonic components frequencies do not coincide with the exciting frequencies. Further elimination of each second order odd multiplier ($OddOdd$) enables, in addition, to separate the third order harmonic components. Such signals were proposed in (Evans and Rees, 1999) and are denoted in the literature by No Interharmonic Distortion (NID).

2.4 Simulation Results

In order to compare the excitations mentioned in Section 2.3 and to study how their time - frequency properties influence the impedance spectrum accuracy, a single Bio-Impedance relaxation model has been simulated. The system has

been modeled with a three parameter equivalent electrical circuit where the parameters are given by C_m = 9.75 (nF), R_e = 120 (Ω) and R_i = 30 (Ω), representative of a myocardium tissue electrical impedance measurement. Figure 2.11 shows the impedance frequency response which is given by:

$$Z(s) = \frac{R_e R_i C_m s + R_e}{(R_e + R_i) C_m s + 1} \tag{2.20}$$

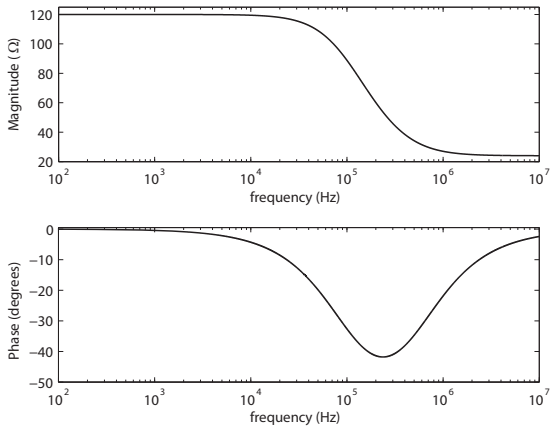

Figure 2.11: Impedance magnitude (top) and phase (bottom) frequency response simulated.

Twenty-one excited frequencies log-odd distributed have been considered in the frequency band from 1 kHz up to 1 MHz. Input and output noise disturbance, $n_u(t)$ and $n_y(t)$ respectively, have been considered in the model and are assumed to be additive, mutually independent and Gaussian distributed with zero mean and standard deviation of 0.01. Hence,

$$\begin{aligned} u(t) &= u_0(t) + n_u(t) \\ y(t) &= y_0(t) + n_y(t) \end{aligned} \tag{2.21}$$

Impedance spectrum $Z_0(k)$ is the mean impedance spectrum magnitude calculated using eq. 2.7. Figure 2.12 shows the impedance plot obtained from the data when using the excitations compared to the theoretical model (see eq. 2.20). It shows that MLBS data are more affected by the presence of the output noise at low frequencies than at high frequencies. In contrast to the MLBS, the chirp excitation fits better at high frequencies than the MLBS. However, the chirp data are dispersive at low frequencies. This is due to the up-chirp excitation focus all the excitation energy at high frequencies. To solve this, others

chirp excitation should be considered (i.e. exponential chirp). In any case, the impedance spectrum is more accurate when using the DIBS or the multisine excitations than when using the chirp or the MLBS excitations. Figure 2.12

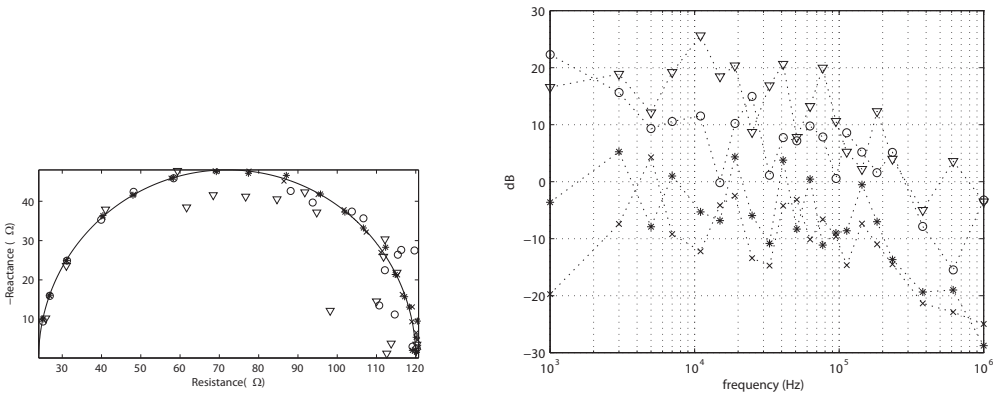

Figure 2.12: Accuracy on the estimated impedance plot with respect to the model (−) considering input-output disturbances (left); resultant impedance spectrum variance σ_Z^2 (right); MLBS ($\triangledown$), chirp ($\bigcirc$), DIBS ($*$) and flat multisine ($\times$).

(right) shows the impedance spectrum variance σ_Z^2, which is the result of calculating the averaged impedance spectrum variance given by eq. 2.7. Figure 2.12 (right) highlights the importance of choosing the excitation in order to obtain reliable measurements. As a result of tis choice, it can be obtained a difference from 10 dB to 20 dB on the impedance spectrum accuracy.

2.5 Experimental results

In order to experimentally compare the results previously mentioned, all excitations were applied to measure a dummy RC circuit impedance. The merit figure used to compare them is the Noise-to-Signal Ratio (NSR) (see eq. 2.7). Two scenarios were considered, first, exciting with the energy limited to 0.35 V_{rms} (see Figure 2.13), and second, exciting with a peak amplitude limitation of 1 V and 25 mV (see Figure 2.14).

2.6 Discussion

As an alternative to periodic Chirp excitation, a modified chirp pulse excitation proposed in (Min et al., 2010) is stated to be the optimal excitation for obtain-

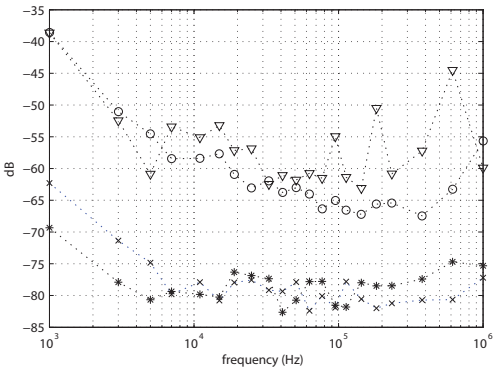

Figure 2.13: Noise-to-Signal Ratio (NSR) with an energy constraint to 0.35 V_{rms}; MLBS ($\triangledown$), chirp ($\circ$), DIBS ($*$) and multisine ($\times$).

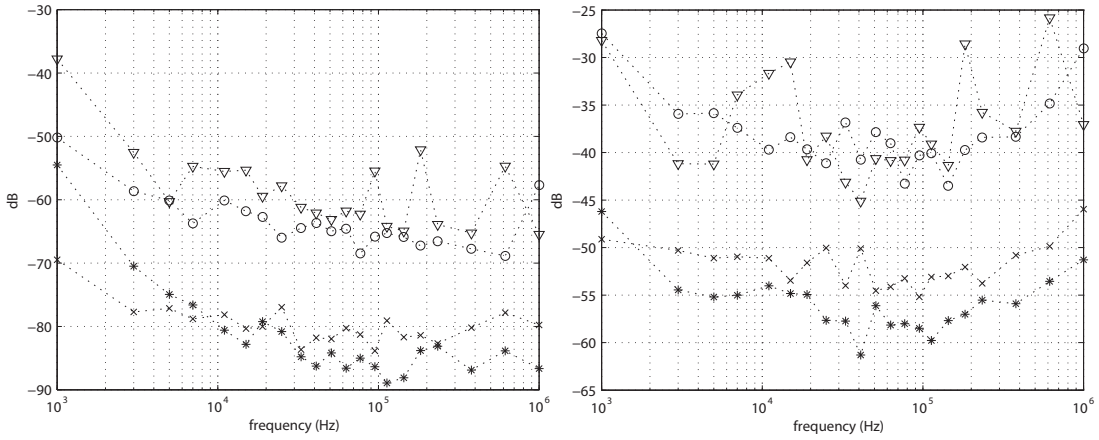

Figure 2.14: Noise-to-Signal Ratio (NSR) with peak value constraint to 1 V (left) and 25 mV (right); MLBS ($\triangledown$), chirp ($\circ$), DIBS ($*$) and multisine ($\times$).

ing the most accurate impedance spectrum. The author claims that "Thanks to unique properties of the chirp function, it is possible to meet the needs for spectrum bandwidth, measurement time, and Signal to Noise Ratio so that the most accurate impedance spectrogram is obtained" is not true. According to the author, this statement is based on the fact that by modifying the excitation bandwidth and its time duration the authors "maximize the amount of information derived from the data of spectral measurements". However, no mathematical solution neither experimental results are provided to support the validity of any of the previously mentioned statements.

Regarding to the first statement, the suggested use of any of the chirp fractional periods rather than full periods should be avoided if accurate impedance spectrum measurements are desired. The use of fractional excitation periods is a well-known source of errors because of a misuse of an excitation. This may affect not only the accuracy on the impedance spectrum estimates due to the introduced leakage effect, but also will cause a serious loss of information on the measured system. This loss of information results into a bad Signal-to-Noise Ratio at certain frequencies that are poorly excited (Simon and Schoukens, 2000). While the leakage effect can be taken into account in the signal processing (Schoukens et al., 2006), the bad SNR due to the loss of information cannot be compensated in any way. Moreover, the simulation and experimental results shown in Section 2.4 and Section 2.5 proof that chirp excitation is far from having the optimal power spectrum as long as the impedance spectrum accuracy is the optimality criteria. When the measurement is limited by the energy applied to the system, Figure 2.13 shows that the MLBS and the chirp excitations have about 20 dB worse impedance spectrum Noise-to-Signal Ratio than the DIBS and the multisine excitations. As shown in Figure 2.14, this trend is the same when the peak value excitation is the design constraint. In this case, the DIBS and the multisine excitations obtain better impedance spectrum accuracy than the MLBS and the chirp with independence of the excitation peak amplitude value.

Referring to the second statement, the way to design an optimal excitation that maximizes the amount of information from the measurements is much more sophisticated than just modifying the excitation spectral content by changing the excitation time duration. The optimal excitation design is based on the Fisher information matrix as shown in (Ng et al., 1977; Schoukens and Pintelon, 1990; Goodwin et al., 2006), where the prior knowledge of the system to measure must be considered. As shown in (Sanchez et al., 2011b), given an impedance model structure with unknown parameters, the impedance spectrum accuracy depends on the identification procedure used. Then, if the estimator

is a Maximum Likelihood Estimator (MLE), its covariance matrix asymptotically reaches the Cramer–Rao (CR) lower bound. Since the elements of the Fisher matrix are directly related to the system parameters variance (Goodwin et al., 2006, 2007), minimizing the covariance matrix is in practice the same as maximizing the information for a given input excitation.

Like chirp excitation, Maximum Length Binary Sequences (MLBS) are another broadband excitation candidate used in (Schneider, 1996; Sun et al., 2007a,b). Its major disadvantage is that a great deal of power is spread over unwanted frequencies. Moreover, the impedance spectrum accuracy may be improved without compromising the measurement time, providing that the excitation could be designed to concentrate the signal power in a discrete set of frequencies like the DIBS signals do.

An approach for designing the optimal multisine excitation for impedance spectroscopy measurements was presented in (Popkirov and Schindler, 1993; Popkirov and Schlinder, 1994). The authors suggested that the multisine fundamental's amplitudes should be designed following the impedance spectrum magnitude measured. However, it has been shown in (Sanchez et al., 2011b,a) that the multisine amplitude distribution that maximizes the impedance spectrum accuracy should focus the excitation energy close to the central frequency. Designing the multisine amplitudes following the impedance frequency response provides less scattering data at low frequencies at the cost of getting dispersive points at the central frequencies and high frequencies.

This page intentionally left blank.

King Arthur: I am, and this is my trusty servant Patsy. We have ridden the length and breadth of the land in search of knights who will join me in my court at Camelot. I must speak with your lord and master.
Soldier: What? Ridden on a horse?
King Arthur: Yes!
Soldier: You're using coconuts!
King Arthur: What?
Soldier: You've got two empty halves of coconut and you're bangin' 'em together.
King Arthur: So? We have ridden since the snows of winter covered this land, through the kingdom of Mercia, through...
Soldier: Where'd you get the coconuts?
King Arthur: We found them.
Soldier: Found them? In Mercia? The coconut's tropical!
to be continued...

-Monty Python and the Holy Grail (1974)

3

A Novel Approach for Impedance Spectrum Estimation: the Local Polynomial Method

In this chapter, the problem of determining the frequency response of time-varying systems under the influence of transients is studied on the basics of the Local Polynomial Method (LPM) described in (Schoukens et al., 2009b; Pintelon et al., 2010a,b). An introduction related to the LPM theory within an Output Error (OE) framework is presented in Section 3.2. The solution to the Error-In-Variables (EIV) model is presented in Section 3.2.2. The processing and measurement principles are validated through a set of simulations shown in Section 3.3. The application of the LPM for healthy myocardium tissue electrical impedance characterization within the cardiac-cycle is presented in Paper B.

3.1 Introduction

Measuring the Electrical Bio-Impedance (EBI) stationary behavior of a biological time-varying system is not sufficient in all the cases. Although the non-stationary behavior of the impedance signal has information about the tissue

activity during time, this information has been usually underestimated in all those studies based on frequency-sweep EIS. In these cases, the time-varying information was usually removed from the impedance signal by averaging the spectral data measuring several realizations.

The requirement that needs to be satisfied in order to obtain the impedance spectrum non-stationary behavior is to acquire several frequencies in a short measuring time. However, measuring in a short time leads to loose impedance spectrum accuracy and the low excited frequencies are prone to be corrupted by the leakage influence when measuring within a non steady-state conditions. If this is the case, the lower the excited frequency is, the more the impedance frequency response from the exact value will differ. Smoothing windows are commonly used to mitigate these errors. Also interpolation methods are applied in the frequency domain to reduce leakage errors (Ferrero and Salicone, 2010). Figure 3.1 shows an example of the transients effect in time over a current $i(t)$ impedance measurement. Both signals are each one a period of a two consecutive periodic multisine measurement. As it can be observed, the initial samples of the first period measured contain the system transient state response.

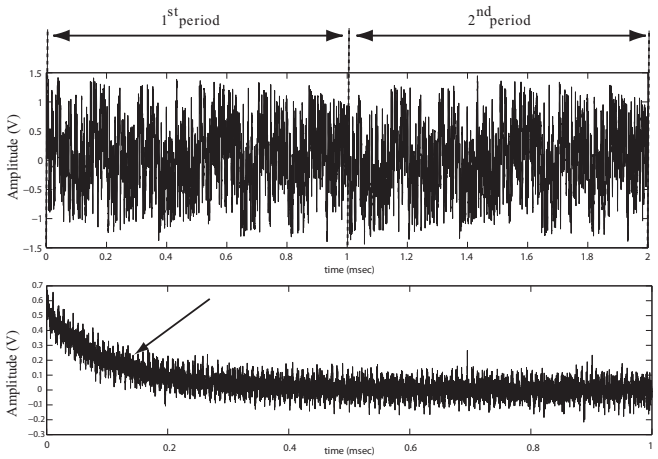

Figure 3.1: Two consecutive periods of a log-odd multisine excitation (top); difference between periods are due to the transients and noise error sources (bottom).

As shown in Figure 3.2, if the impedance spectrum is then determined in the frequency domain using the Fast Fourier Transform (FFT), these transients errors appear as leakage. As a result of this leakage, the low frequency excited lines can no longer be distinguished and this results in errors at the impedance spectrum estimation at low frequencies. However, this does not occur in the

example considered if only the second period is used. In practice, the time the transient takes to expire depends on the application, so it could happen that more than just a single period was corrupted by its influence. Thus, the easiest

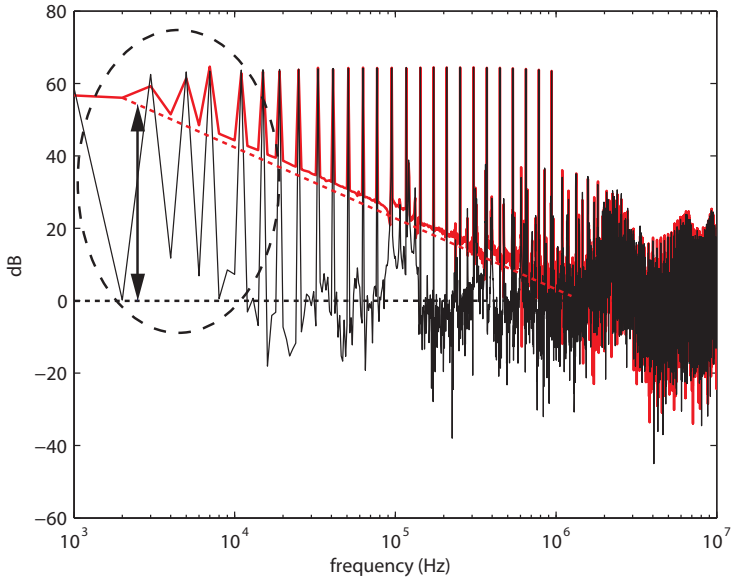

Figure 3.2: First (red) and second period (black) current spectra; the noise floor of the steady-state current measurement is approximately between 60 and 70 dB below the noise floor of the current corrupted by the leakage. As a consequence of the leakage, the effective Signal-to-Noise Ratio (SNR) is reduced.

solution to avoid leakage is to measure the system steady state response. That means wait until the transient expires. Nevertheless, this is not always affordable. Another option consists in increasing the number of samples acquired. This yields more accurate measurements but at the cost of increasing both the measuring time and the hardware resources. The classical way to reduce leakage errors and to mitigate their effect over the frequency response estimation is based on using spectral windows. Windowing the spectrum using Hanning window rejects leakage efficiently and reduces the noise floor. Recent advanced signal processing techniques, the so called Local Polynomial Method (LPM) (Pintelon et al., 2010a,b), achieve better leakage reduction than the windowing methods (Harris, 1978; Schoukens et al., 2009b). Moreover, the mentioned method do no compromise the measuring time if low order polynomials are considered for the analysis. However, there is an increase of the spectral processing complexity.

3.2 The Local Polynomial Method (LPM)

There are techniques to reduce the leakage and to enforce the accuracy of the the spectral data. The assumptions for using the Local Polynomial Method (LPM) are three: (1) the system frequency response is smooth enough in frequency so it can locally be approximated by a p^{th} order polynomial, (2), the leakage error source is produced by the transient, so it is assumed to be smooth in the frequency domain and that it can be described using a polynomial too, and (3), the excitation is not smooth (i.e. multisine). When observing that the leakage contribution to the spectrum, $T(\omega)$, is smooth over the frequency, it becomes clear that it can be removed from the steady-state contributions.

3.2.1 Output Error (OE) framework

The Output Error (OE) model (see Figure 3.3) considers that the measured output voltage spectrum $V(\Omega_k)$ is the combination of the input current spectrum $I(\Omega_k)$ multiplied by the impedance frequency response $G(\Omega_k)$, with an output additive transient $T(\Omega_k)$ and noise $N(\Omega_k)$ error sources:

$$V(k+r) = G(k+r)\,I(k+r) + T(k+r) + N(k+r) \tag{3.1}$$

where $\Omega_k = j\omega_k$ with $2\pi k f_s/N$ and f_s sampling frequency. The impedance

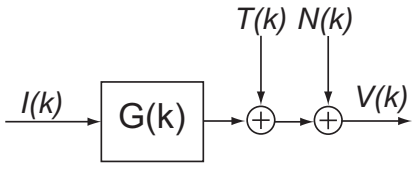

Figure 3.3: Input - output discrete Fourier transform (DFT), $I(k)$ and $V(k)$, and the frequency response $G(k)$ at the excited frequency k. $T(k)$ is the additive transient and $N(k)$ the additive noise source.

spectrum $G(k)$ and the transient frequency response $T(k)$ are both smooth and parametrized using a p^{th} order polynomial at the excited bins, k. Considering the neighboring spectral points $r = [-n, ..., -1, 0, 1, ..., n]$ it follows that:

$$\begin{aligned} G(k+r) &= G(k) + a_1 r + \ldots + a_p r^p \\ T(k+r) &= T(k) + t_1 r + \ldots + t_p r^p \end{aligned} \tag{3.2}$$

where $V, I \in C_{2n+1,1}$. The impedance spectrum is then estimated by solving the set of equations:

$$V = K_I \theta \tag{3.3}$$

with respect to the unknowns $\theta \in C_{2p+2,1}$:

$$\theta = \left[G\left(k\right), a_1, \ldots, a_p, T\left(k\right), t_1, \ldots, t_p\right]^H \tag{3.4}$$

where the superscript H is the Hermitian (complex conjugate) operator and $K_I \in C_{2n+1,2p+2}$ is given by:

$$K_I = \begin{pmatrix} I\left(k-n\right) & \ldots & -n^p \cdot I\left(k-n\right) & 1 & -n & \ldots & -n^p \\ \vdots & \ldots & \vdots & \vdots & \vdots & \ldots & \vdots \\ I\left(k+n\right) & \ldots & n^p \cdot I\left(k+n\right) & 1 & n & \ldots & n^p \end{pmatrix} \tag{3.5}$$

The Least Square (LS) solution is a possible way to solve over-determined set of equations if $2n+1 > 2p+2$ (Golub and Van Loan, 1980), namely:

$$\hat{\theta} = \left(K_I^H K_I\right)^{-1} K_I^H V \tag{3.6}$$

Figure 3.4 illustrates the steps to compute the EBI spectrum according to eq. 3.6. This implicitly assumes that the additive noise, $N\left(k\right)$, is independent over

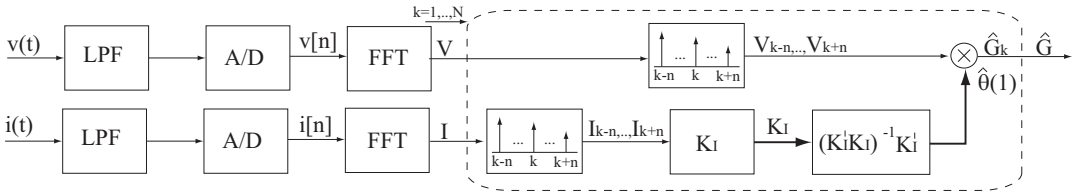

Figure 3.4: Scheme of an impedance measurement system implementing the OE-LPM solution; Upper case characters I and V denote the Fourier transformed time variables current i and voltage v measured; Dotted line highlights the additional signal processing for calculating the LPM solution; the LPM needs to be calculated for each excited frequency (N).

the frequency k and has a white power spectrum in the considered frequency range $(\omega_{k-r} \ldots \omega_{k+r})$. This Least Square solution has a high computational cost. Fortunately, since K_I only depends on the current spectrum $I\left(k\right)$, it only needs to be computed at the excited frequencies. Hence, if the inputs are known beforehand, then the Least Square problem can be precomputed using i.e. the Moore-Penrose algorithm or the Singular Value Decomposition.

3.2.2 Errors-In-Variables (EIV) framework

The fast LPM measurement principle exploits the properties of the Error-In-Variables (EIV) framework (see Figure 3.5) to compute the Least Square (LS)

solution considering the voltage and current measurements. As a result, the impedance spectrum can be estimated multiplying small matrices, which considerably reduce the processing time compared to the general LPM solution. Consider the system shown in Figure 3.5 with current $i(t)$ and voltage $v(t)$ measurements:

$$\begin{aligned} v(t) &= v_0(t) + n_v(t) \\ i(t) &= i_0(t) + n_i(t) \end{aligned} \tag{3.7}$$

where all observations are corrupted by additive zero-mean measurement noise sources $n_i(t)$ and $n_v(t)$ and the reference signal, $r(t)$, is exactly known. The

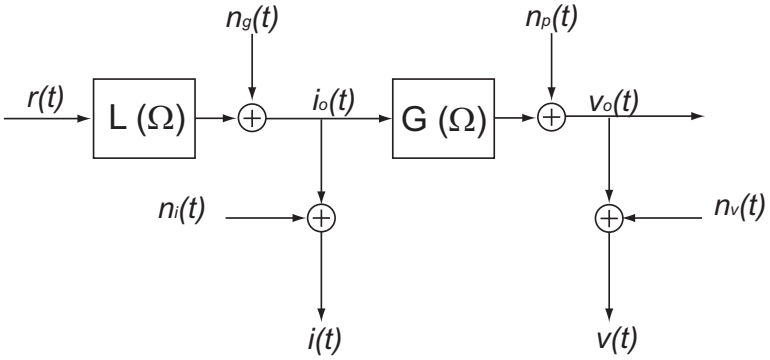

Figure 3.5: Measurement of the impedance spectrum of a system $G(\Omega)$ within an Errors-In-Variables (EIV) stochastic framework in open loop setup. $r(t)$ is the known reference signal loaded into the Arbitrary Waveform Generator (AWG); $n_g(t)$, $n_p(t)$, $n_i(t)$ and $n_v(t)$ are, respectively, the generator, process, current measurement and voltage measurement noise sources; $L(\Omega)$ is the actuator transfer function.

model that yields to unbiased estimates of the input/output spectra, $I(k)$ and $V(k)$ respectively, and the noise covariance matrix if the input/output observations are noisy is known as Error-In-Variables (EIV) problem. If the reference signal $r(t)$ is known, the model to solve is:

$$Z(k) = G_{RZ}(\Omega_k) R(k) + H_{RZ}(\Omega_k) E(k) + T_{RZ}(\Omega_k) \tag{3.8}$$

with $G(\Omega)$ and $H(\Omega)$ the system and noise transfer functions, $E(k)$ the unobserved white noise sources, and $T(\Omega)$ the leakage terms. The system transfer function G_{RZ} is a column vector (relating R towards the input I and the output V), T_{RZ} is a column vector containing the transients and H_{RZ} represents the noise sources obtained by filtering two independent noise sources (hence E is a

column vector) using a 2x2 filter matrix H_{RZ}:

$$Z(k)_{2n+1,2} = \begin{bmatrix} V(k) \\ I(k) \end{bmatrix}, \quad G_{RZ}(\Omega_k) = \begin{bmatrix} G_{RV}(\Omega_k) \\ G_{RI}(\Omega_k) \end{bmatrix} \tag{3.9}$$

and $V_{RZ}(k) = H_{RZ}(\Omega_k) E(k)$ models that part of the input – output DFT spectra that does not depend on the reference signal. Although the noise transfer function, $H(\Omega)$, and noise source, $E(k)$, can be identified separately, we will work with their noise covariance matrices.

A consistent estimates of the impedance spectrum $G(\Omega_k)$ and the noise covariance matrix of the input-output current and voltage spectra, $I(k)$ and $V(k)$ respectively, can be obtained from the frequency response function $\hat{G}_{RZ}(\Omega_k)$ and the noise covariance matrix estimate $\hat{C}_{V_{RZ}}$ using the following equation:

$$\hat{G}(\Omega_k) = \hat{G}_{RV}(\Omega_k) \hat{G}_{RI}^{-1}(\Omega_k) \tag{3.10}$$

$$Cov\left(\begin{bmatrix} V(k) \\ I(k) \end{bmatrix}\right) = \hat{C}_{V_{RZ}}(k) \tag{3.11}$$

3.2.3 Implementation

In contrast to the general Local Polynomial Method (LPM) described in Section 3.2, the fast LPM precomputes the matrices defined in eq. 3.5 and eq. 3.6 with respect to the reference signal $R(k)$. If the reference is a multisine signal with all its exciting frequencies on the DFT grid with at least n zero lines around the excited frequency k, then $K_R \in C_{2n+1,p+2}$. Then, it is possible to reduce the polynomial model for the system towards the matrix K_R where only the transient parameters need to be estimated in addition to G(k):

$$K_R = \begin{pmatrix} 0 & 1 & -n & -n^2 & \dots & -n^p \\ 0 & 1 & -(n-1) & -(n-1)^2 & \dots & -(n-1)^p \\ \vdots & \vdots & \vdots & \vdots & \dots & \vdots \\ R_k & 1 & 0 & 0 & \dots & 0 \\ \vdots & \vdots & \vdots & \vdots & \dots & \vdots \\ 0 & 1 & (n-1) & (n-1)^2 & \dots & (n-1)^p \\ 0 & 1 & n & n^2 & \dots & n^p \end{pmatrix} \tag{3.12}$$

Note that if there is not at least n zero lines around the excited frequency k_i, the neighbor excited lines $k_{i\pm1}$ must be considered in the analysis. This means that the size of the K_R matrix given in eq. 3.12 $(2n+1, p+2)$ is no longer valid.

The general expression of $K_R \in C_{2n+1,2p+2}$ must then be calculated according to eq. 3.5.

Consider the matrix $K_P \in C_{2+p,2n+1}$ to compute the Least Square solution:

$$K_P = \left(K_R^H K_R\right)^{-1} K_R^H \tag{3.13}$$

In this case, the K_P matrix only depends on the reference $R(k)$ and not in the measurements. For that reason, the K_P matrix can be precomputed in advance for all the excited frequencies Ω_k. As a result of this, the run-time computation time for estimating the impedance spectrum is drastically reduced. That is because the only additional operations needed to be computed are small matrix products that aim to determine the frequency response from the reference to the current and voltage, $\hat{G}_{RI}(\Omega_k)$ and $\hat{G}_{RV}(\Omega_k)$ respectively, namely:

$$\begin{aligned} \hat{\theta}_{RI_{p+2,1}} &= K_{P_{p+2,2n+1}} I_{2n+1,1} \\ \hat{\theta}_{RV_{p+2,1}} &= K_{P_{p+2,2n+1}} V_{2n+1,1} \end{aligned} \tag{3.14}$$

The division of both is the unbiased estimate of the impedance frequency response $\hat{G}(\Omega_k)$ (see eq. 3.10). The conceptual block diagram is shown in Figure 3.6.

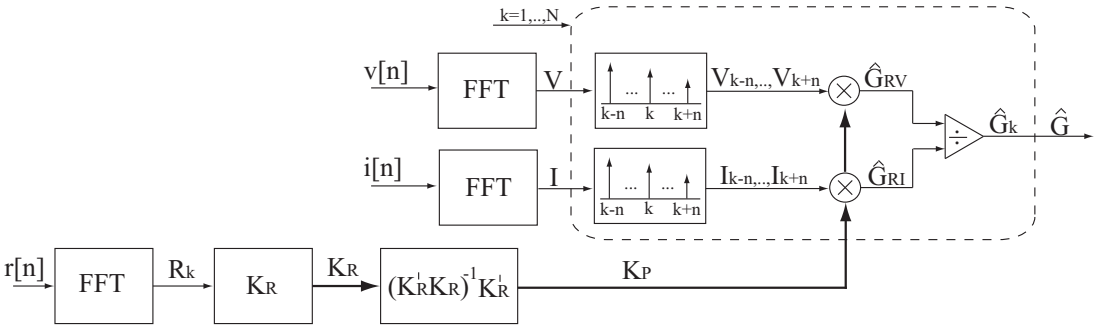

Figure 3.6: Scheme of the fast EIV-LPM implementation. The Least Square matrix solution K_P is calculated using the reference signal and it is stored in the program memory.

The residual errors of the Least Square modeling and the covariance matrix on the estimates can be optionally computed using the projection matrices $K_N \in C_{2n+1,2n+1}$ and $K_{CP} \in C_{2+p,2+p}$ given by:

$$K_N = I_{2n+1,2n+1} - K_R(K_R^H K_R)^{-1} K_R^H \tag{3.15}$$

$$K_{CP} = \left(K_R^H K_R\right)^{-1} \tag{3.16}$$

3.3 Simulation Results

The aim of the simulations is to compare the impedance spectrum accuracy obtained when using Hanning window and the LPM. Two different frequency response functions have been considered in the simulations. To provoke spectral data to be corrupted by leakage, both systems have been excited with a pure random noise excitation. Figure 3.7 and Figure 3.8 show the complex error of the frequency response estimated using the classical spectral windowing methods based on auto/cross correlation using Hanning window and using the Local Polynomial Method ($p = 2$, $n = 3$).

3.3.1 Two Resistors-One Capacitor circuit (2R-1C)

Figure 3.7 (left) illustrates the equivalent electrical circuit and its Nyquist plot. The parameter values used for the simulations are $C = 5$ nF, $R_2 = 130\Omega$ and $R_1 = 150\Omega$, from 1 kHz to 1 MHz. As it can be observed in Figure 3.7 (right), the leakage errors of the LPM are between 50 dB at and 100 dB less than using windows.

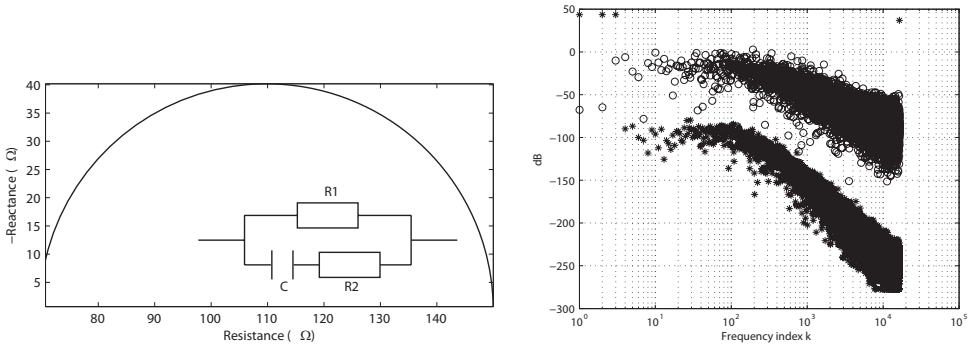

Figure 3.7: Equivalent electrical circuit of the 2R-1C system and its Nyquist plot (left); Complex error between the model and the estimated frequency response using the Hanning window $Z_{2R-1C} - \hat{Z}_{hann}$ (○) and the LPM $Z_{2R-1C} - \hat{Z}_{LPM}$ (∗) (right).

3.3.2 Three Resistors-Two Capacitor circuit (3R-2C)

Figure 3.8 (left) illustrates the equivalent electrical circuit and its Nyquist plot. The model parameters used for the simulations are $C_1 = 10$ nF, $R_1 = 150\Omega$, $C_2 = 5$ nF, $R_2 = 40\Omega$ and $R_3 = 100\Omega$, from 1 kHz to 100 MHz. As shown in Figure 3.8 (right), the leakage errors of the LPM are still about 50 dB to 100

dB below when compared to the Hanning window. This occurs even when the complexity of the model is increased.

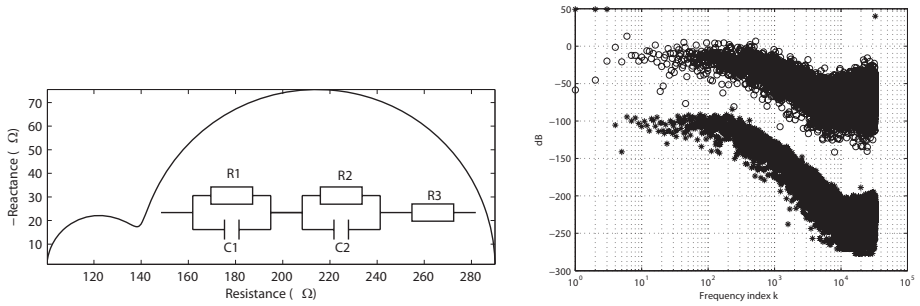

Figure 3.8: Equivalent electrical circuit of the 3R-2C system and its Nyquist plot (left); Complex error between the model and the estimated frequency response using the Hanning window $Z_{3R-2C} - \hat{Z}_{hann}$ (○) and the LPM $Z_{3R-2C} - \hat{Z}_{LPM}$ (∗) (right).

3.4 Processing time

The drawback of this improvement on the impedance spectrum accuracy is the additional computational time added in the data processing after calculating the voltage and current spectra. Because this is a critical issue that concerns many real-time applications, Figure 3.9 illustrates the dependency of the LPM processing time with respect to the neighbour points n and polynomial order p considered and compared to the FFT time processing. As shown in Figure 3.9, the processing time added does not penalize the calculation time for real-time EBI monitoring applications for polynomial orders $p < 20$. Experimental results from the LPM implementation are 150 impedance spectra/second (1 period), 75 impedance spectra/second (two periods), 51 impedance spectra/second (three periods) and 39 impedance spectra/second (four periods). The more periods are considered, the higher impedance spectrum Signal-to-Noise ratio is measured.

The results presented in Paper B have shown that for a given low order polynomial ($p = 2$) and considering a small number of neighbor points ($n = 3$), the impedance spectrum Signal-to-Noise Ratio is improved 20 dB to 50 dB compared to Hanning window at frequencies below 10 kHz.

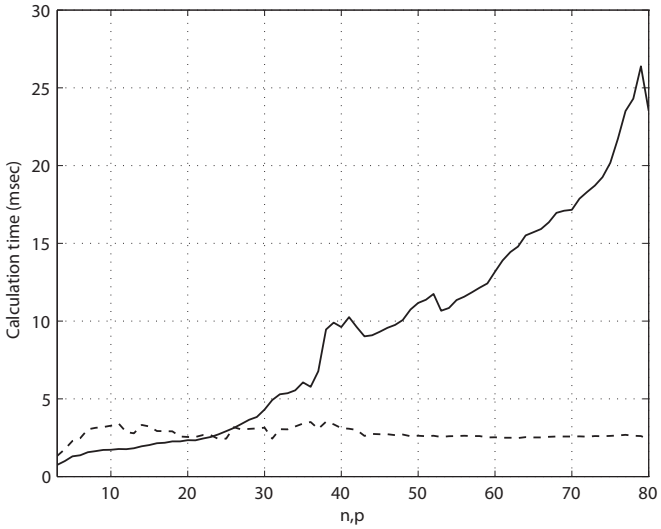

Figure 3.9: Time required for the calculation of the voltage V and current I spectra (−−) (40 Msamples, 2 periods) compared to the calculation time needed for the calculation of the fast LPM implementation (exciting frequencies N=26)(−). Results obtained with a Personal Computer (Intel Core Duo, 2.10 GHz) running Matlab R2009b.

This page intentionally left blank.

King Arthur: What do you mean?
Soldier: Well, this is a temperate zone.
King Arthur: The swallow may fly south with the sun or the house martin or the plover may seek warmer climes in winter, yet these are not strangers to our land?
Soldier: Are you suggesting coconuts migrate?
King Arthur: Not at all. They could be carried.
Soldier: What? A swallow carrying a coconut?
King Arthur: It could grip it by the husk!
Soldier: It's not a question of where he grips it! It's a simple question of weight ratios! A five ounce bird could not carry a one pound coconut.
King Arthur: Well, it doesn't matter. Will you go and tell your master that Arthur from the Court of Camelot is here?.

-Monty Python and the Holy Grail (1974)

4

A preliminary study on minimally invasive *in-vivo* human lung tissue characterization using Impedance Spectroscopy

This chapter presents the preliminary results of a study that is being performed at the moment of finishing this thesis. It would be a new application of non-stationary EBI measurements, aiming to minimally invasive *in-vivo* characterization of human lung tissue pathologies using an electronic biopsy based on Electrical Impedance Spectroscopy. In Section 4.1 there is an introduction to the motivation of this research study. Sections 4.4 and 4.5 describe the methods and materials used. Next, Sections 4.6 and 4.7 describe in more detail the four-wire electrical impedance measurement system and the issues related to the measuring system calibration and characterization. Finally, Section 4.9 presents the preliminary results of the measurement campaign carried out in collaboration with the Pneumology Service from the Hospital Santa Creu i Sant Pau (HSCSP).

4.1 Introduction

Respiratory diseases include diseases of the lung, pleura, bronchial tree, trachea, upper respiratory tract and of the respiratory muscles and nerves.They are a common and important cause of illness and death among the population. According to the report from the *Instituto Nacional de Estadistica*[1], in 2008, the respiratory diseases represented 11,4% of the causes of mortality in Spain. The same pattern remained of mortality was mantained in 2009. The three leading causes were diseases of circulatory system (31.2%), tumors (27.3%) (see Figure 4.1) and respiratory diseases (11.2%).

No screening is currently applied to detect lung cancer, so the majority of cases are diagnosed after the appearance of symptoms and a radiological study (usually by Computed Tomography (CT)) showing a pulmonary lesion. Although the symptoms and radiological tests results may indicate the presence of cancer, the diagnosis needs histological analysis for confirmation and cell type identification. The cells from lungs are usually obtained from sputum or by more invasive 3dures such us bronchoscopy. Bronchoscopy consists in the introduction, usually through the nose, of a flexible tube to explore and obtain samples from the airways. The procedure is performed under local anesthesia and sedation to avoid patient's discomfort by a lung specialist. Several samples can be obtained from bronchoscopies: bronchial wash and aspiration, bronchial brush, transbronchial needle aspiration, and biopsies from both, bronchial mucosa and lung parenchyma (transbronchial) The transbronchial biopsy procedure is performed using a tiny forceps that are passed through a channel of the bronchoscope into the lungs. While the patient is exhaling, the pulmonologist collects a small sample of the lung tissue. Due to the uncertainty in the biopsy, it is necessary to repeat this step until several samples are collected for tissue analysis. In some occasions, X-rays fluoroscopy imaging in real-time is performed during the bronchoscopy to help in directing the forceps to the area to be scanned in the lungs.

4.2 Motivation

Experimental evidence show that cancerous skin lesions have different electrical properties compared with non-cancerous lesions or normal tissue (Aberg et al., 2003, 2004). Therefore, cancerous ones may be differentiated from non-cancerous lung tissue lesions by comparing the tissue passive electrical prop-

[1] http://www.ine.es/

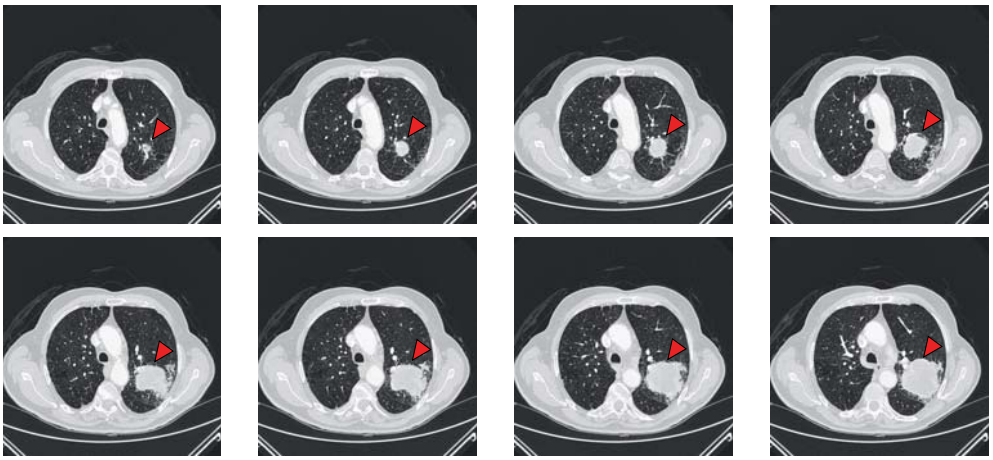

Figure 4.1: Computed Tomography (CT) scanning images corresponding to patient 1467834; red arrow indicates the presence of a cancerous mass in the left lung (right side of the image).

erties with those of the surrounding healthy tissues. The aim of this study is twofold: (1), to investigate whether using Electrical Impedance Spectroscopy may improve the biopsy diagnosis procedure, and (2), whether EIS technique can differentiate between pathological lung or not. As a preliminary task, this Chapter presents a feasibility study on how the previously developed technique presented in Chapter 2 and Chapter 3, can help to improve the lung tissue characterization at the moment of the biopsy, including the dynamic behavior.

4.3 Measurement Protocol

After the patient's approval, the bronchoscopy was performed in a special room designated for such procedures. During the procedure, midazolam sedative and local anesthetic like lidocaine was used to anesthetise the mucous membranes of the pharynx, larynx and trachea. The patients were continuously ECG monitored during the procedure. The flexible bronchoscope was inserted with the patient in a supine position entering through the left nose hole. Once the bronchoscope was inserted into the upper airway, the vocal cords were inspected. The bronchoscope advanced to the trachea and further down into the bronchial system. Each area was visually inspected as the bronchoscope went through it. Right and left lungs were inspected. Depending on the medical staff decision, tissue could be sampled using a biopsy (transbronchial biopsy) using real-time x-ray guidance.

4.4 Methodology description

The research performed is a cross-sectional population study where, in the absence of previously *in-vivo* published data, n has been estimated to 40 subjects. The subjects will be divided into 4 groups according to the presumptive diagnosis by chest CT scan: emphysema, malignancy, pulmonary fibrosis or healthy parenchyma (i.e. hemoptysis with normal CT). It is estimated that with 10 subjects per group of patients selected according to basic radiological patterns that were clearly differentiated each other seems to be a reasonable number of individuals to find differences between them. To be selected for participation individuals were referred to the medical unit. The inclusion criteria consists on the indication for bronchoscopy study of respiratory disease, in the opinion of the medical responsible for the patient, the pulmonary function study and blood gases at rest and air, CT chest scan, age superior to 18 years and the patient signed informed consent. Patients were excluded when previous history of poor tolerance to respiratory endoscopy, the inability to 8-second apnea, any psychiatric disorder or limitation to collaboration (i.e. including language problem or socio-cultural among others), notorious instability (i.e respiratory failure) prior to bronchoscopy in the opinion of bronchoscopist assume an increased risk for the patient to be included in the study.

4.5 Materials

In order to perform the EIS measurements, we employed a tetrapolar probe catheter (Bard Electrophysiology VIKING, 400041) with 115 cm length and a diameter of 1.65 mm (5F). The probe has a line of isolated polymer with four platinum electrodes separated by a distance of 2 mm and placed in the distal shaft section. For safety reasons, a patient front-end previously designed to accomplish the safety regulation for medical devices (EN 60601-1) (Ramos et al., 2004) was used. The maximum patient auxiliary rms current injected by the system in working condition to the patient is 90uA. The catheter was placed inside the alveolus trough the same interior channel of the bronchoscope used for the biopsy (see Figure 4.2).

4.5.1 Measurement System

The measurement system shown in Figure 4.2 is composed by three devices:

1. the isolated front end, which is an optically isolated patient interface battery power provided including two ECG channels and the impedance front end.

2. the core of the measurement system based on a PXI system.

3. an analog-optical interface front end to connect the PXI with the front end.

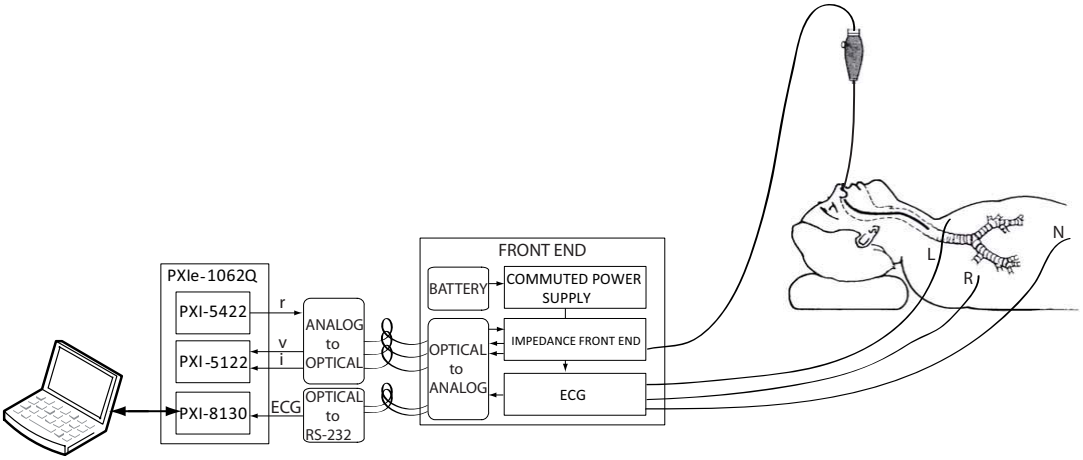

Figure 4.2: Block diagram description of the system setup at the hospital operation room; a nasal bronschoscopy is performed to the patient to observe the lobar and segmental bronchi.

4.5.1.1 Electrocardiogram (ECG) board

The ECG measurement system has two channels (internal and external). The external channel has conventional features: a band pass frequency response with cut-off frequencies of 0.5 Hz or 0.05 Hz (selectable) for the high pass filter and and 100 Hz for the low pass filter. The instrumentation amplifier for both ECG channels uses the AD627. External ECG signal is sampled at 945 Hz with a 12-bit A/D converter integrated in the microcontroller (ADuC 812). This board has also two channels available for the absolute and differential temperature measurement that are not used in this application. The PXI controller (PXIe-8130) is in charge of the acquisition of the ECG signal. It does so using an optical-RS232 modem within the ECG board available in the front end.

4.5.1.2 Electrical Bio-Impedance measurement system

The system includes an embedded controller PXIe-8130, a 2 channel high-speed digitizer card PXIe-5122 (100Ms/s, 64MB/channel, 14bits) and an arbitrary waveform card PXI-5422 (200Ms/s, 32MB, 16 bits). While the AWG (PXI-5422) generates the multisine excitation $r(t)$, the two channel digitizer (PXIe-5122) acquires voltage $v(t)$ and current $i(t)$ system response. The Electrical Bio-Impedance is estimated in the frequency domain using the Fast Local Polynomial Method described in Section 3.2.2.

The excitation $r(t)$ is converted into an optical signal with the optical-analog interface connected to the PXI. Then, it is converted again into an electrical signal inside the front end. The voltage $v(t)$ and current $i(t)$ signals, which are optically transmitted from the front end to the optical-electrical interface, are filtered (cut-off frequency 10 MHz) and acquired with the digitizer card.

4.6 Measurement System characterization

This section describes the measurements performed in the laboratory using experimental models to verify the functionality of the measurement system and to evaluate its main specifications and limitations.

4.6.1 Impedance measurement errors: linearity

In order to determine the system linearity, we measured ten resistors (5% tolerance) with the nominal values of 100 Ω, 150 Ω, 200 Ω, 270 Ω, 360 Ω, 470 Ω, 670 Ω, 750 Ω, 820 Ω and 910 Ω. Terminals HPOT with HCUR and LPOT wit LCUR were shorted respectively. The impedance spectrum magnitude $|Z|$ and phase φ were calibrated using the 100 Ω resistor as a reference values at the following exciting frequencies:

$$\begin{aligned} f\,(kHz) \;=\; & 10, 13, 17, 21, 26, 32, 39, 48, 59, 72, 87, 105, 127, 154, \\ & 186, 224, 270, 325, 391, 470, 565, 679, 816, 981 \end{aligned} \tag{4.1}$$

according to the following equations:

$$\begin{aligned} |Z| &= \frac{|Z_{measured}|}{|Z_{100\Omega}|} \cdot R_{100\Omega} \\ \varphi &= \varphi_{measured} - \varphi_{Z_{100\Omega}} \end{aligned} \tag{4.2}$$

Figure 4.3 shows on the x-axis the real value of the resistors measured with a multimeter (with a accuracy of 0.1%) and on the y-axis the real part of the

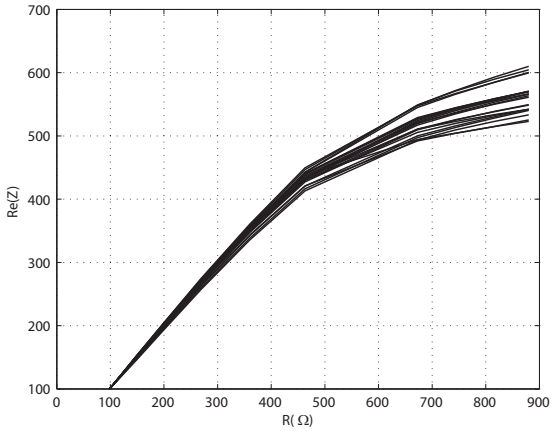

Figure 4.3: Real value of the resistors measured vs. the resistance of the impedance measured using a multisine excitation at the excited frequencies.

impedance for each frequency. As shown in Figure 4.3, the input impedance that can be measured by the front end is not higher than 400 Ω. From 400 Ω, the front end stage goes into saturation and its response ceases to be linear. Nevertheless, it is not expected to measure lung tissue impedance above this value. It it could seem that the system presents a stronger non-linearities behavior at high frequencies than at low frequencies within the linear region ($100\Omega < \Re e\,(Z) < 400\Omega$). Nevertheless, this effect is due to the input capacitance from the differential amplifier used to measure the voltage $v\,(t)$ between HPOT and LPOT terminals, which has higher influence at high frequencies than low frequencies.

4.6.2 Characterization of the system frequency response

In order to characterize the contribution of system nonlinearities to the Electrical Bio-Impedance, the patient has been replaced by a 100 Ω resistor (5% tolerance) with two configurations. In the first configuration, the resistor was connected directly to the Impedance front end box without connecting the catheter. In the second configuration, the resistor was connected to the tip of catheter directly to the electrodes and then the catheter connected to the Front End. Figure 4.6 shows the frequency response function of front end (−−) and including the catheter (−). The use of the catheter modifies both the magnitude and phase. In fact, the way the phase is modified is somewhat unpredicatable since it is highly sensitive to several uncontrollable factors. These factors are:

1. the position of the catheter influences on the effective capacitive coupling from the catheter cable to ground.

2. how the phase is affected by the crosstalk between the catheter cables remains unclear.

3. the length of catheter introduced into the lungs is not constant, so the capacitive coupling catheter-patient will vary with each patient measured.

For all these mentioned reasons, it is preferable to obtain knowledge about the nonlinear and noise source levels than calibrating the measured phase with accuracy.

4.6.2.1 Study of the Non-Linearities: measuring the Best Linear Approximation (BLA)

Consider a Error-In-Variables (EIV) framework (noisy input/output measurements), as shown in Figure 4.4, where G_{BLA} is the Best Linear Approximation

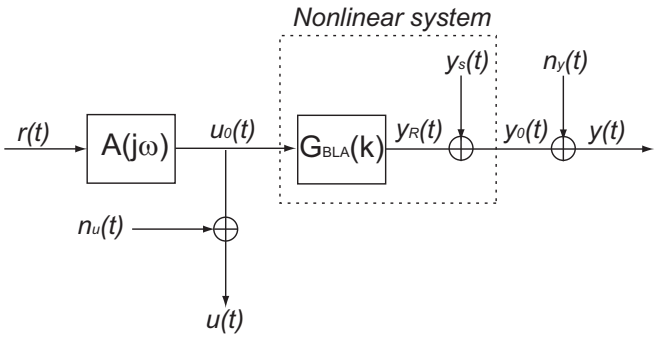

Figure 4.4: Measurement of the Best Linear Approximation of a nonlinear system within an Error-In-Variables (EIV) stochastic framework in open loop setup. $A\left(j\omega_k\right)$ is the linear actuator transfer function. $r\left(t\right)$ is the known reference signal loaded into the Arbitrary Waveform Generator (AWG). $y_s\left(t\right)$ is the stochastic nonlinear noise source contribution that depends on the input power spectrum and the even and odd nonlinearities. $n_u\left(t\right)$ and $n_y\left(t\right)$ are, respectively, the input and output noise sources.

(BLA) related to the Linear Time Invariant (LTI) behavior of a nonlinear system (Schoukens et al., 2002, 2008, 2009a). The nonlinear system is modeled by a linear system G_{BLA} and a output additive nonlinear source of noise $y_s\left(t\right)$. Then, the spectrum from the input/output measurements, $U\left(k\right)$ and $Y\left(k\right)$ re-

spectively, can be projected to the reference spectra $R(k)$, giving:

$$\begin{aligned} U_R(k) &= \frac{U(k)}{R(k)} = U_{R0}(k) + \frac{N_U(k)}{R(k)} \\ Y_R(k) &= \frac{Y(k)}{R(k)} = Y_{R0}(k) + \frac{Y_S(k)}{R(k)} + \frac{N_Y(k)}{R(k)} \end{aligned} \tag{4.3}$$

with

$$\begin{aligned} U_{R0}(k) &= A(j\omega_k) \\ Y_{R0}(k) &= G_{BLA}(j\omega_k)\, U_{R0}(k) \end{aligned} \tag{4.4}$$

where $A(j\omega_k)$ is the linear actuator transfer function. The phases of $U_{R0}(k)$ and $Y_{R0}(k)$ are only dependent on both the actuator transfer function and the Best Linear Approximation. Then, it follows from eq. 4.3 that the projected input/output DFT spectra, $U_R(k)$ and $Y_R(k)$, can be averaged over both the P periods and the M realizations in the measurement scheme of the robust method presented in Figure 4.5.

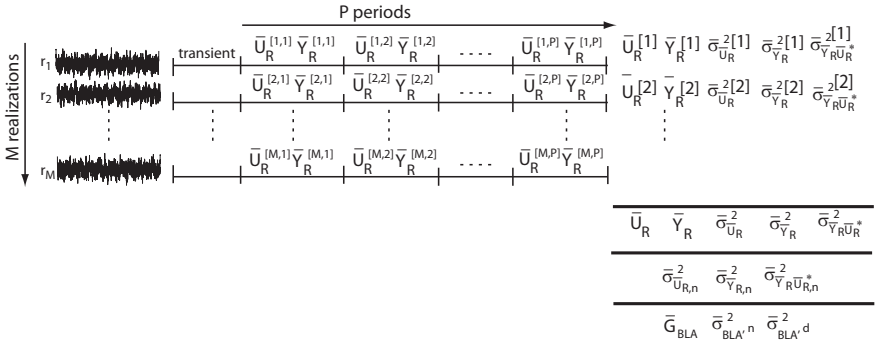

Figure 4.5: Robust method scheme for estimating the Best Linear Approximation G_{BLA} of a nonlinear system within an Error-In-Variables (EIV) framework, where M different random phase multisine excitations $r_i(t)$ are used.

The steps to estimate the Best Linear Approximation shown in Figure 4.6 are:

1. Calculate the input, output and reference DFT spectra of each period.
2. Calculate the projected input/output spectra of the m^{th} realization and p^{th} period with respect the reference (see eq. 4.3)
3. Perform a variance analysis of the set of the projected input/output DFT spectra (see Appendix eq. B.1)
4. Calculate the uncertainty of the frequency response function (see Appendix eq. B.2, eq. B.3 and eq. B.4)

The robust method experiment has consisted on ten realizations (M=10) and ten periods (P=10). For each realization, the excitation consisted on a different random phase multisine (1 ms, Fs 20 MHz). The exciting frequencies are shown in eq. 4.1. All the random phases multisines were designed to have the same energy. As shown in Figure 4.7 (left), the contribution of the non-linear dis-

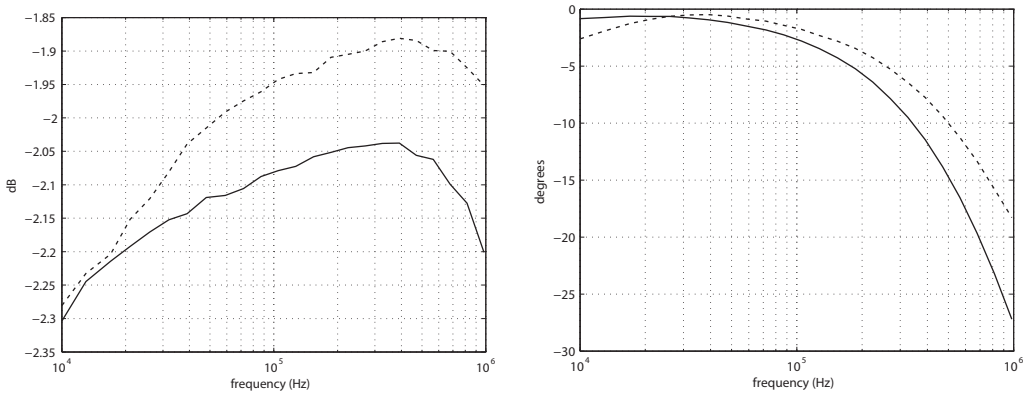

Figure 4.6: Magnitude (left) and phase (right) of the Best Linear Approximation frequency response function when measuring a 100 Ω resistor directly connected to the front end (−−) and including the catheter (−).

tortions introduced by the front end are negligible in comparison to the system noise variance. However, Figure 4.7 (right) shows that the catheter increases the stochastic non-linear distortions. However, the non-linearities introduced are not critic since they remain about 50 dB below the level of the frequency response.

4.7 Measurement system calibration

The impedance measurement technique used is a 4-wire and is made available through the electrodes in the catheter, described in Section 4.5, which is connected to the impedance front end. These electrodes are arranged at the end of the catheter and its configuration is as follow: Low Current (LC), Low Potential (LP), High Potential (HP) and High Current (HC), respectively.

4.7.1 Finite Elements Model (FEM) simulation

In order to perform the calibration of the EBI measurement system, different conductivity solutions were simulated using COMSOL Multiphysics.

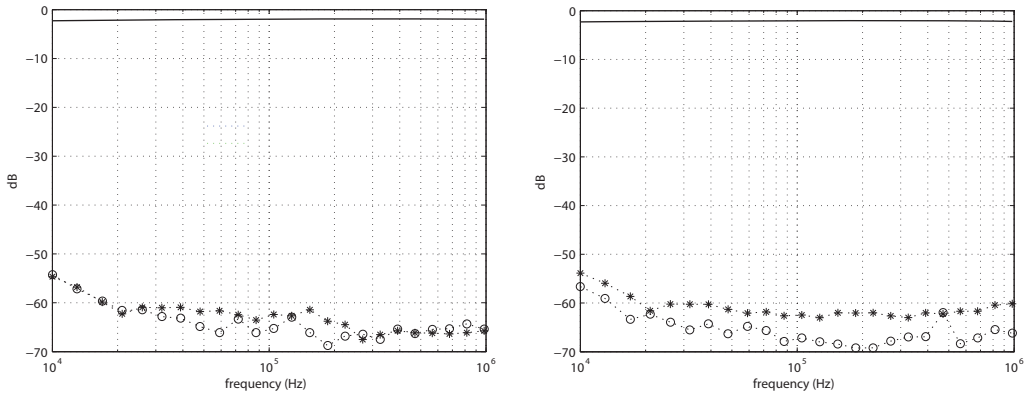

Figure 4.7: Magnitude of the Best Linear Approximation $\overline{G}_{BLA}(j\omega)$ (−), noise variance $\overline{\sigma}^2_{\overline{G}_{BLA},n}(j\omega)$ (○) and total variance $\overline{\sigma}^2_{\overline{G}_{BLA}}(j\omega)$ ($*$) which includes the noise and non-linear distortions of the front end (left) and including the catheter (right).

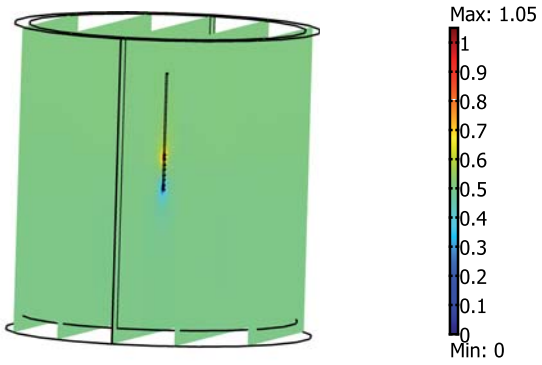

Figure 4.8: Distribution of the electrical potential at the electrode.

According to the measuring system calibration procedure, the catheter was simulated to be placed in the middle of a plastic cylinder containing the calibration solution. The catheter was modeled by the composition of eight piled cylinders representing each of the electrodes and the polyurethane space between them. The final assembly produced a Finite Element (FE) mesh with a limited number of elements simulated under 3D quasi-static/electric AC/DC conditions.

4.8 Simulation Results

Figure 4.9 shows the expected lung's Electrical Bio-Impedance according to the model described in (Gabriel et al., 1996) given by:

$$\varepsilon(\omega) = \varepsilon_\infty + \sum_{m=1}^{4} \frac{\Delta\varepsilon_m}{1 + (j\omega\tau_m)^{1-\alpha_m}} + \frac{\sigma_i}{j\omega\varepsilon_0} \tag{4.5}$$

where ε_0 is the permittivity of free space and ω the angular frequency. Equation 4.5 models the dielectric data as a summation of 4-Cole-Cole expression (see eq. 1.27) using the electrical conductivity σ_i and permittivity ε_m values available from the study of Carrara, N.[2]. The tissue resistivity ρ^* is calculated as the inverse of the complex conductivity σ^* as shown in eq. 1.12 and eq. 1.16 using eq. 4.5. Considering the electrodes having negligible dimensions and being surrounded by a mass of infinite size, the lung's impedance measured with 4-wire technique can be approximated by the following expression:

$$Z^*(\omega) \approx \frac{\rho^*(\omega)}{4\pi d} \tag{4.6}$$

where d is the distance between electrodes. For the catheter used (see Section 4.5), the distance between the center of the electrodes is $d = 3.5mm$. In the range of β dispersion, it is possible to observe that there is a significant difference in the magnitude when lungs are inflated or deflated. The inflated lungs show a higher impedance modulus than the deflated lungs due to the fact that the electrical conductivity decreases as much as the lungs are inflated with oxygen. Moreover, the major phase relaxation is expected to occur close to 1 MHz in both cases, where the inflated present a lower phase value than when deflated. Nevertheless, the interpretation of these data must be carefully done: part of the data were obtained from *ex-vivo* experimental measurements while

[2] http://niremf.ifac.cnr.it/tissprop/

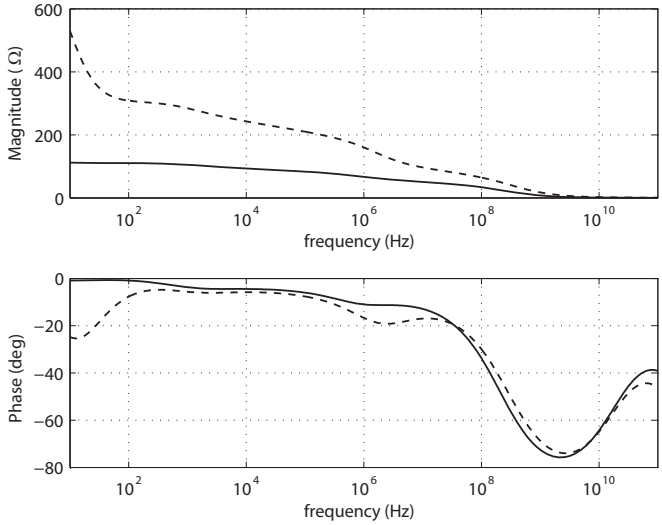

Figure 4.9: Magnitude (top) and phase (bottom) characteristic frequency response simulated when inflated (−−) and deflated (−).

other were obtained from extrapolating experimental data. However, a clinical *in-vivo* trial is a more complex scenario. The Electrical Bio-Impedance signal will be under the influence of the heartbeat, due to the lung's blood perfusion, and the breathing cycle because of the lungs' ventilation. Furthermore, the Electrical Bio-Impedance signal is expected to change depending on the physiological state of the lung and on the specific characteristics of the injury being measured. In addition, noise and artifacts due to complications during the procedure could influence the measurements. Stridor and dyspnea resulting from laryngeal edema, laryngospasm, or even bronchospasm are some examples of complications that are reflected into artifacts in the signal.

4.9 Experimental Results

Figure 4.10 illustrates an electronic biopsy of the lung tissue. The frequencies used in the electronic biopsy method (see Section 4.6) are chosen to obtain information about the clinical tissue relevant properties, such as tissue composition of intra and extra-cellular environments, cell shape and size.

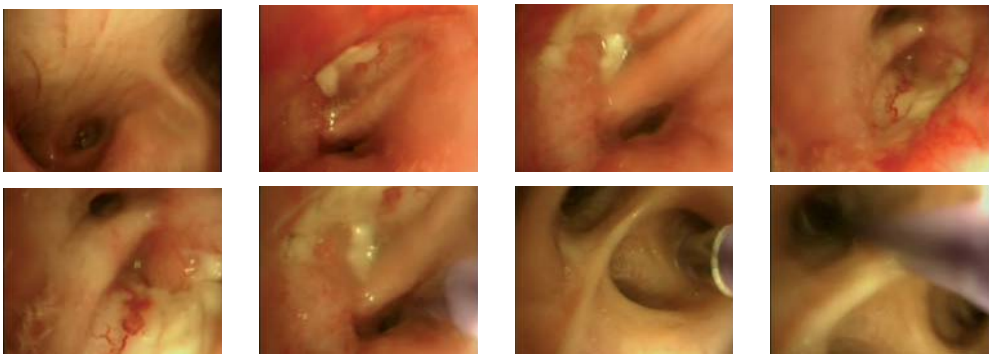

Figure 4.10: Catheter placed inside the alveolus, in contact with the lung parenchyma (alveolar tissue) (patient 430021).

4.9.1 Influence of the ventilatory signal

The major drawback when measuring Electrical Bio-Impedance in humans is the significant variation of the ventilation rate, which occurs unexpectably. In contrast to the Electrical Bio-Impedance magnitude, the phase is not subjected to the modulation of respiration. Figure 4.11 (left) illustrates the changes in time when the lungs are inflated or deflated.

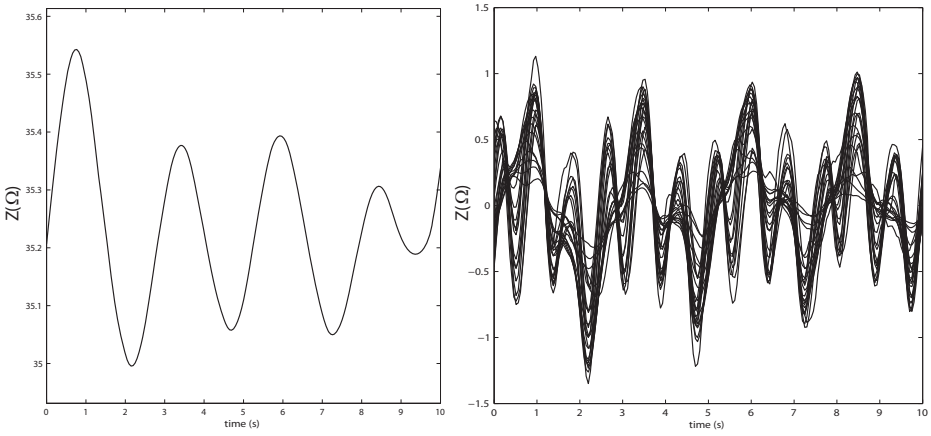

Figure 4.11: Detail of the time-variation of the impedance magnitude at 186 kHz due to the influence of the pulmonary ventilation (left); Variation in time of the impedance spectrum magnitude at the exciting frequencies due to the cardiac-cycle (right) (patient 1109639).

4.9.2 Influence of the cardiac signal

If no respiration is present in the Electrical Bio-Impedance signal, i.e. during an apnea, the effect of heartbeat would be the only source of disturbance on the measurement. To achieve this situation, the patients should be able to maintain a prolonged apnea. As shown in Figure 4.11 (right), the speed of acquisition of the measurement system and the fast Local Polynomial Method performance enables to appreciate the cardiac and pulmonary related changes in the impedance spectrum. Thus, it is not longer necessary to cause an apnea to patients.

4.10 Discussion

The preliminary data analyzed suggests that the electrical impedance magnitude changes depending on whether or not the tissue has an injury. It holds promise on helping histopathologists to diagnose lung cancer. At the moment of writing the thesis, 9 patients were already measured, which presented different lung tissue pathologies. A first observation is that there is a significant difference in the EBI magnitude when lungs are inflated or deflated. Moreover, differences in the impedance spectrum magnitude suggest that impedance can be a valid indicator to distinguish lung tumors from healthy tissue.

Being the Electrical Impedance technique a non-invasive approach, the patient would have a fast and accurate method of detection, undergo less pain, less bleeding and have greater comfort. However, further research is needed and more patients should be studied. The Electrical Bio-Impedance data should be correlated with histologist analysis to reveal real evidences for being used as a clinical diagnosis tool.

This page intentionally left blank.

Dr. Frederick Frankenstein: You know, I'm a rather brilliant surgeon. Perhaps I can help you with that hump.
Igor: What hump?.

-Young Frankstein (1974)

5 Conclusions and Guidelines for future research

5.1 Conclusions

The general conclusions and topics of research presented in this thesis cover the challenges to measure time-varying Electrical Bio-Impedance (EBI) measurements. On one hand, the optimal multisine excitation for short time Electrical Impedance Spectroscopy (EIS) has been designed. More precisely, this research activity has contributed to overcome the problem of measuring in a reduced measuring time with energy restrictions. A formal approach for designing the optimal time and frequency multisine excitation has been presented enabling the impedance spectrum accuracy to be maximized. Following, there is a detailed list focusing on the relevant results obtained:

- The main advantage that multisine offers with respect to rest of excitations studied for EBI measurements is that the user has the flexibility to directly specify the power spectrum (amplitudes and frequencies). The phases must be selected to minimize its Crest Factor in order to reduce the overall amplitude span of the excitation. This is done while main-

taining the same level of power in the exciting fundamental frequencies. Unlike other excitations such as chirp, the user has total control of the multisine time/frequency domain properties. This can be an advantage or not, depending on the user experience.

- To identify the most suitable excitation we have to consider that in most of the applications taking measurements in a limited set of exciting frequencies is enough. The reason why the complete spectrum is not necessary is due to the EBI frequency behavior. EBI responses decrease monotonically with frequecny and only a few samples are needed to be fitted into a model. Considering as constraints the measuring time and the maximum peak value of the excitation, the impedance spectrum accuracy is the cost function that should be considered. The optimal time/frequency domain multisine excitation has been designed by minimizing its Crest Factor (CF) and the Cramer-Rao (CR) lower bound respectively. The published results shown in Paper A have contributed to understand the relation between the multisine exciting frequency distribution, the amplitude power spectrum and the impedance spectrum accuracy. Next list summarizes the most relevant results obtained so far:
  - Not all the exciting frequencies and excitation amplitude power spectrum contribute in the same way to increase the impedance spectrum accuracy.
  - The EBI dispersion function maximum value when exciting an equally-spaced or logarithmic frequency distributions is higher than when exciting with a custom frequency distribution that places more excited frequencies close to the central frequency of the impedance relaxation.
  - The equally-spaced and the logarithmic frequency distributions require a higher number of exciting frequencies to obtain the same impedance spectrum accuracy as the previously mentioned custom frequency distribution.
  - The impedance spectrum accuracy is more sensitive to the excitation amplitude power spectrum than to the excited frequency distribution used.
  - The variance of the impedance spectrum is higher close to the central frequency of the relaxation than in other frequencies.
  - Increasing the number of exciting frequencies contributes to minimize the impedance spectrum variance. However, its influence is reduced

as the number of exciting frequencies becomes sufficiently large. As a result, a discrete power spectrum like multisine with enough exciting frequencies provides the same information as a full grid power spectrum exciting all the spectral lines.

On the other hand, a novel spectral estimation method has been used for impedance spectrum estimation based on the Local Polynomial Method (LPM). The presented method overcomes the limitations of current spectral estimation methods when processing data under the influence of transients. Through simulations, it has been shown that leakage error's influence on the EBI is efficiently rejected at low frequencies. This enables to achieve a greater accuracy on the impedance spectrum than classical spectral methods based on windows (between 50 dB and 100 dB more accurate depending on the polynomial order considered). Furthermore, the additional calculation time of the fast LPM version is negligible compared to the computation time of the Fast Fourier Transform (FFT) for low order polynomials (only 1ms). Moreover, the improvement in the accuracy is about 30 dB at 1 kHz and 50 dB at 3 kHz (p=10).

This knowledge has been applied to two different measurement campaigns within the collaboration from Hospital Santa Creu i Sant Pau (HSCSP) for *in-vivo* human lung and myocardium tissue electrical impedance characterization. The results obtained have shown successful evidences when measuring under the influence of non-stationary behavior such as the pulmonary ventilation and the cardiac-cycle time variation, being the cardiac-cycle the most restrictive application.

5.2 Guidelines for future research

In a view of the work presented in this thesis, various research lines can be established.

- To study the changes of the myocardium electrical impedance in time during an acute ischemic process. Simultaneous acquisition of pressure wave in the ventricle and its correlation with the Cole parameters will help to interpret the results.

- Increase the number of patients with the aim of achieving a significant population sample to enable the study of the *in-vivo* passive electrical properties of lungs with different diseases. Segmenting the population according to the type of lung disease, with the aim of studying whether

EIS can help to perform better biopsies and to characterize different lung tissue states.

- To study the dependency of the impedance model parameters accuracy considering the frequency. The goal is to identify whether exists frequencies band or not where it is preferable to measure in order to minimize the variance of the impedance model parameters.
- To apply the broadband EIS technique for non-invasive monitoring of the engineered tissue developed within the research projects described in Section 0.1. Develop tissue state multivariate estimators. This could include time-frequency behavior information for *in-vitro* detection of stem cell differentiation and *in-vivo* engineered heart tissue viability for cardiac tissue regeneration.
- To study the possibility to extend the range of applications of broadband EIS based on multisine to microfluidics, Electrical Impedance Tomography (EIT) and Electrochemical field.

References

P. Aberg, I. Nicander, U. Holmgren, P. Geladi, and S. Ollmar. Assessment of skin lesions and skin cancer using simple electrical impedance indices. Technical Report 3, Division of Medical Engineering, Karolinska Institutet, Huddinge, Sweden, 2003.

P. Aberg, I. Nicander, J. Hansson, P. Geladi, U. Holmgren, and S. Ollmar. Skin cancer identification using multifrequency electrical impedance–a potential screening tool. *IEEE transactions on bio-medical engineering*, 51(12):2097–102, December 2004. ISSN 0018-9294. doi: 10.1109/TBME.2004.836523.

B. Alberts, A. Johnson, J. Lewis, M. Raff, K. Roberts, and P. Walter. *Molecular Biology of the Cell*. Garland Science, 2002. ISBN 0815332181.

N. Bao, J. Wang, and C. Lu. Recent advances in electric analysis of cells in microfluidic systems. *Analytical and bioanalytical chemistry*, 391(3):933–42, June 2008. ISSN 1618-2650. doi: 10.1007/s00216-008-1899-x.

E. Beller and D. J. Newman. An L1 Extremal Problem for Polynomials. *Proceedings of the American Mathematical Society*, 29(3):474–481, 1971.

R. Bragos, R. Blanco-Enrich, O. Casas, and J. Rosell. Characterisation of dynamic biologic systems using multisine based impedance spectroscopy. *IEEE Proceedings on Instrumentation and Measurement Technology Conference*, (1):44–47, 2001. doi: 10.1109/IMTC.2001.928785.

B. H. Brown. Electrical impedance tomography (EIT): a review. *Journal of medical engineering & technology*, 27(3):97–108, 2003. ISSN 0309-1902. doi: 10.1080/0309190021000059687.

K. C. Cheung, M. Di Berardino, G. Schade-Kampmann, M. Hebeisen, A. Pierzchalski, J. Bocsi, A. Mittag, and A. Tárnok. Microfluidic impedance-based flow cytometry. *Cytometry. Part A : the journal of the International*

Society for Analytical Cytology, 77(7):648–66, July 2010. ISSN 1552-4930. doi: 10.1002/cyto.a.20910.

J. Cinca, M. Warren, A. Rodríguez-Sinovas, M. Tresànchez, A. Carreño, R. Bragos, O. Casas, A. Domingo, and J. Soler-Soler. Passive transmission of ischemic ST segment changes in low electrical resistance myocardial infarct scar in the pig. *Cardiovascular research*, 40(1):103–12, October 1998. ISSN 0008-6363.

K. S. Cole and R. H. Cole. Dispersion and Absorption in Dielectrics I. Alternating Current Characteristics. *The Journal of Chemical Physics*, 9(4):341, 1941. ISSN 00219606. doi: 10.1063/1.1750906.

S.C. Creason and D.E. Smith. Fourier transform faradaic admittance measurements II. Ultra-rapid, high precision acquisition of the frequency response profile. *Journal of Electroanalytical Chemistry*, 40(1):A1–A5, 1972. ISSN 0022-0728.

C. Evans and D. Rees. Nonlinear distortions and multisine signals. I. Measuring the best linear approximation. *IEEE Proceedings on Instrumentation and Measurement Technology Conference*, 2(3):1038–1046, 1999.

M. A. Fallert, M. S. Mirotznik, S. W. Downing, E. B. Savage, K. R. Foster, M. E. Josephson, and D. K. Bogen. Myocardial electrical impedance mapping of ischemic sheep hearts and healing aneurysms. *Circulation*, 87(1):199–207, January 1993. ISSN 0009-7322.

A. Ferrero and S. Salicone. A fast frequency-domain interpolation method for the evaluation of the frequency and amplitude of spectral components. *2010 IEEE Instrumentation & Measurement Technology Conference Proceedings*, 60(5):6–11, 2010. doi: 10.1109/IMTC.2010.5488212.

S. Gabriel, R. W. Lau, and C. Gabriel. The dielectric properties of biological tissues : II . Measurements in the frequency range 10 Hz to 20 GHz. *Physics in Medicine and Biology*, 41:2251–2269, 1996.

E Gersing. Impedance spectroscopy on living tissue for determination of the state of organs. *Bioelectrochemistry and Bioenergetics*, 45:145–149, 1998.

K. R. Godfrey. Introduction to binary signals used in system identification. *IEEE Conference on Control 1991.*, pages 161–166, 1991.

K. R. Godfrey, H. A. Barker, and A. J. Tucker. Comparison of perturbation signals for linear system identification in the frequency domain. *IEEE Proceedings on Control Theory and Applications*, 146(6):535–548, 1999. doi: 10.1049/ip-cta.

K. R. Godfrey, A. H. Tan, H. A. Barker, and B. Chong. A survey of readily accessible perturbation signals for system identification in the frequency domain. *Control Engineering Practice*, 13(11):1391–1402, 2005. ISSN 09670661. doi: 10.1016/j.conengprac.2004.12.012.

G.H. Golub and C.F. Van Loan. An analysis of the total least squares problem. *SIAM Journal on Numerical Analysis*, 17(6):883–893, 1980. ISSN 0036-1429.

G. Goodwin, C. Rojas, J. Welsh, and A. Feuer. Robust optimal experiment design for system identification. *Automatica*, 43(6):993–1008, June 2007. ISSN 00051098. doi: 10.1016/j.automatica.2006.12.013.

G. C. Goodwin, J. Welsh, A. Feuer, and M. Derpich. Utilizing prior knowledge in robust optimal experiment design. In *14th IFAC Symposium on System Identification*, pages 1358–1363, 2006.

O. Grauhan, J. Müller, C. Knosalla, T. Cohnert, H. Siniawski, H. D. Volk, E. Fietze, W. Kupetz, and R. Hetzer. Electric myocardial impedance registration in humoral rejection after heart transplantation., February 1996. ISSN 1053-2498.

P. Guillaume, J. Schoukens, R. Pintelon, and I. Kollar. Crest-factor minimization using nonlinear Chebyshev approximation methods. *IEEE Transactions on Instrumentation and Measurement*, 40(6):982–989, 1991. ISSN 00189456. doi: 10.1109/19.119778.

F.J. Harris. On the use of windows for harmonic analysis with the discrete Fourier transform. *Proceedings of the IEEE*, 66(1):51–83, 1978. ISSN 0018-9219. doi: 10.1109/PROC.1978.10837.

A. Hartov, R. A. Mazzarese, F. R. Reiss, T. E. Kerner, K. S. Osterman, D. B. Williams, and K. D. Paulsen. A multichannel continuously selectable multifrequency electrical impedance spectroscopy measurement system. *IEEE Transactions on Biomedical Engineering*, 47(1):49–58, 2000.

A. Horner and J. Beauchamp. A genetic algorithm-based method for synthesis of low peak amplitude signals. *Acoustical Society of America*, 99(1):433–443, 1996.

O. L. Hubin, R. Pintelon, and A. Hubin. Detection and evaluation of measurement noise and stochastic non-linear distortions in electrochemical impedance measurements by a model based on a broadband periodic excitation. *Journal of Electroanalytical Chemistry*, 576(1):65–72, 2005. ISSN 15726657. doi: 10.1016/j.jelechem.2004.09.029.

M. Ichise, Y. Nagayanagi, and T. Kojima. Application of pseudo-random signals and cross-correlation techniques in electroanalytical chemistry. *Journal of Electroanalytical Chemistry*, 49(2):187–198, 1974. ISSN 0022-0728.

U. G. Kyle, I. Bosaeus, A. D. De Lorenzo, P. Deurenberg, M. Elia, J. M. Gómez, B. L. Heitmann, L. Kent-Smith, J.-C. Melchior, M. Pirlich, H. Scharfetter, A. M. W. J. Schols, and C. Pichard. Bioelectrical impedance analysis–part I: review of principles and methods. *Clinical nutrition (Edinburgh, Scotland)*, 23 (5):1226–43, October 2004. ISSN 0261-5614. doi: 10.1016/j.clnu.2004.06.004.

H. Lee, D. E. Rivera, and H. D. Mittelmann. Constrained Minimum Crest Factor Multisine Signals for "Plant-Friendly" Identification of Highly Interactive Systems. *13th Internation Federation of Automation Control Symposium on System Identification*, 2003.

F. Lisdat and D. Schäfer. The use of electrochemical impedance spectroscopy for biosensing. *Analytical and bioanalytical chemistry*, 391(5):1555–67, July 2008. ISSN 1618-2650. doi: 10.1007/s00216-008-1970-7.

J. Malmivuo and R. Plonsey. *Bioelectromagnetism: Principles and Applications of Bioelectric and Biomagnetic Fields*. Oxford University Press, 1995.

E. T. McAdams and J. Jossinet. Tissue impedance : a historical overview. *Physiological Measurements*, 16:A1–A13, 1995.

F. Mellert, K. Winkler, C. Schneider, T. Dudykevych, A. Welz, M. Osypka, E. Gersing, and C. Preusse. Detection of (Reversible) Myocardial Ischemic Injury by Means of Electrical Bioimpedance. *IEEE transactions on bio-medical engineering*, (c), June 2010. ISSN 1558-2531. doi: 10.1109/TBME.2010.2054090.

M. Min, A. Kink, R. Land, T. Parve, and I. Rätsep. Modification of pulse wave signals in electrical bioimpedance analyzers for implantable medical devices. *IEEE Engineering in Medicine and Biology Society*, 3:2263–6, January 2004. ISSN 1557-170X. doi: 10.1109/IEMBS.2004.1403658.

M. Min, U. Pliquett, T. Nacke, A. Barthel, P. Annus, and R. Land. Signals in bioimpedance measurement : different waveforms for different tasks. *13th International Conference on Electrical Bioimpedance and the 8th Conference on Electrical Impedance Tomography*, 17(7):181–184, 2007.

M. Min, U. Pliquett, T. Nacke, A. Barthel, P. Annus, and R. Land. Broadband excitation for short-time impedance spectroscopy. *Physiological measurement*, 29(6):S185–92, 2008. ISSN 0967-3334. doi: 10.1088/0967-3334/29/6/S16.

M. Min, R. Land, T. Paavle, T. Parve, and P. Annus. Broadband spectroscopy of a dynamic impedance. In *Internation Conference of Electrical Bioimpedance*, number 1, pages 1–4, 2010.

H. D. Mittelmann, G. Pendse, D. E. Rivera, and H. Lee. Optimization-based design of plant-friendly multisine signals using geometric discrepancy criteria. *Computational Optimization and Applications*, 38(1):173–190, 2006.

H. Morgan, T. Sun, D. Holmes, S. Gawad, and N.G. Green. Single cell dielectric spectroscopy. *Journal of Physics D: Applied Physics*, 40(1):61–70, January 2007. ISSN 0022-3727. doi: 10.1088/0022-3727/40/1/S10.

T. Nacke, A. Barthel, J. Friedrich, M. Helbig, J. Sachs, M. Schäfer, P. Peyerl, and U. Pliquett. A new hard and software concept for impedance spectroscopy analysers for broadband process measurements. *International Federation for Medical and Biological Engineering*, 17:194–197, 2007.

T. Ng, R. L. Payne, and G. C. Goodwin. On maximal accuracy estimation with output power constraints. *IEEE Transactions on Automatic Control*, 133(x): 133–134, 1977.

O. T. Ogunnika, M. Scharfstein, R. C. Cooper, H. Ma, J. L. Dawson, and S. B. Rutkove. A Handheld Electrical Impedance Myography probe for the assessment of neuromuscular disease. *Conference of the IEEE Engineering in Medicine and Biology Society.*, 2008:3566–9, January 2008. ISSN 1557-170X. doi: 10.1109/IEMBS.2008.4649976.

M. E. Orazem and B. Tribollet. Electrochemical Impedance Spectroscopy. *Annual review of analytical chemistry Palo Alto Calif*, 3(1):207–29, 2008. ISSN 19361335. doi: 10.1146/annurev.anchem.012809.102211.

T. Paavle, M. Min, J. Ojarand, and T. Parve. Short-Time Chirp Excitations for Using in Wideband Characterization of Objects : An Overview. In *Electronics Conference (BEC), 2010 12th Biennial Baltic*, pages 253–256, 2010.

R. Pintelon, J. Schoukens, and G. Vandersteen. Frequency domain system identification using arbitrary signals. *IEEE Transactions on Automatic Control*, 42(12):1717–1720, 1997. ISSN 00189286. doi: 10.1109/9.650025.

R. Pintelon, J. Schoukens, G. Vandersteen, and K. Barbé. Estimation of nonparametric noise and FRF models for multivariable systems. Part I: Theory. *Mechanical Systems and Signal Processing*, 24(3):573–595, April 2010a. ISSN 08883270. doi: 10.1016/j.ymssp.2009.08.009.

R. Pintelon, J. Schoukens, G. Vandersteen, and K. Barbé. Estimation of nonparametric noise and FRF models for multivariable systems. Part II: Extensions, applications. *Mechanical Systems and Signal Processing*, 24(3):596–616, April 2010b. ISSN 08883270. doi: 10.1016/j.ymssp.2009.08.010.

U. Pliquett. Fast Impedance Measurements and Non-linear behavior. In *XII International Conference of Electrical Bio Impedance and V Electrical Impedance Tomography*, 2004.

U. Pliquett. Bioimpedance: A Review for Food Processing. *Food Engineering Reviews*, 2(2):74–94, 2010. ISSN 18667910. doi: 10.1007/s12393-010-9019-z.

U. Pliquett and K. Schoenbach. Changes in electrical impedance of biological matter due to the application of ultrashort high voltage pulses. *IEEE Transactions on Dielectrics and Electrical Insulation*, 16(5):1273–1279, 2009. ISSN 10709878. doi: 10.1109/TDEI.2009.5293938.

G. S. Popkirov and F. Schindler. Optimization spectroscopy of the perturbation signal for electrochemical in the time domain impedance. *Reviews in Scientific instruments*, 64(11):3111–3115, 1993.

G. S. Popkirov and R.N. Schlinder. The perturbation signal for fast Fourier transform electrochemical impedance spectroscopy (FFT-EIS). In *Bulgarian Chemical Communications*, pages 459–467, 1994.

J. Pumplin. Low-noise noise. *Acoustical Society of America*, 78(1):100–104, 1985.

J. Ramos, R. Bragos, M.A. Garcia, Y. Salazar, A. Fontova, A. Bayes, J. Cinca, and J. Rosell. Multiparametric measurement system for detection of cardiac graft rejection. In *Proceedings of the 21st IEEE Instrumentation and Measurement Technology Conference (IEEE Cat. No.04CH37510)*, pages 1701–1705. IEEE, 2004. ISBN 0-7803-8248-X. doi: 10.1109/IMTC.2004.1351409.

D. Rees, D.L. Jones, and C. Evans. Practical considerations in the design of multisine test signals for system identification. *Conference Record IEEE Instrumentation and Measurement Technology Conference*, pages 174–179, 1992. doi: 10.1109/IMTC.1992.245155.

B. Rigaud, L. Hamzaoui, M. R. Frikha, N. Chauveau, and J. P. Morucci. In vitro tissue characterization and modelling using electrical impedance measurements in the 100 Hz-10 MHz frequency range. *Physiological measurement*, 16(3 Suppl A):A15–28, August 1995. ISSN 0967-3334.

Y. Rolain, R. Pintelon, and J. Schoukens. Generation and processing of robust periodic excitations. In *Proceedings of the 14th IFAC Symposium on System Identification*, pages 1347–1351, 2006.

Y. Salazar, R. Bragos, O. Casas, J. Cinca, and J. Rosell. Transmural versus nontransmural in situ electrical impedance spectrum for healthy, ischemic, and healed myocardium. *IEEE transactions on bio-medical engineering*, 51 (8):1421–7, August 2004. ISSN 0018-9294. doi: 10.1109/TBME.2004.828030.

B. Sanchez, R. Bragos, and G. Vandersteen. Influence of the Multisine Excitation Amplitude Design for Biomedical Applications using Impedance Spectroscopy. *33rd Annual International Conference of the IEEE EMBS*, (1): 3975–3978, 2011a.

B. Sanchez, G. Vandersteen, R. Bragos, and J. Schoukens. Optimal multisine excitation design for broadband electrical impedance spectroscopy. *Measurement Science and Technology*, 22(11):115601, November 2011b. ISSN 0957-0233. doi: 10.1088/0957-0233/22/11/115601.

M. Schaefer, W. Gross, J. Ackemann, and M. M. Gebhard. The complex dielectric spectrum of heart tissue during ischemia. *Bioelectrochemistry (Amsterdam, Netherlands)*, 58(2):171–80, December 2002. ISSN 1567-5394.

I. Schneider. Broadband signals for electrical impedance measurements of long bone fractures. *Proceedings of the 18th Annual International Conference of the IEEE Engineering in Medicine and Biology Society*, pages 1934–1935, 1996. doi: 10.1109/IEMBS.1996.646327.

J. Schoukens and T. Dobrowiecki. Design of broadband excitation signals with a user imposed power spectrum and amplitude distribution. *IEEE Instrumentation and Measurement Technology Conference*, 2:1002–1005, 1998.

J. Schoukens and R. Pintelon. Design of optimal excitation signals. *IEEE Colloquium on Multifrequency Testing for System Identification*, (02):3/1–3/3, 1990.

J. Schoukens, R. Pintelon, E. van Der Ouderaa, and J. Renneboog. Survey of excitation signals for FFT based signal analyzers. *IEEE Transactions on Instrumentation and Measurement*, 37(3):342–352, 1988.

J. Schoukens, P. Guillaume, and R. Pintelon. Design of Multisine Excitations. *International Conference on Control*, 1:638–643, 1991.

J. Schoukens, R. Pintelon, and Y. Rolain. Broadband versus stepped sine FRF measurements. *IEEE Transactions on Instrumentation and Measurement*, 49 (2):275–278, 2000. ISSN 00189456. doi: 10.1109/19.843063.

J. Schoukens, R. Pintelon, and T. Dobrowiecki. Linear modeling in the presence of nonlinear distortions. *IEEE Transactions on Instrumentation and Measurement*, 51(4):786–792, August 2002. ISSN 0018-9456. doi: 10.1109/TIM.2002.803298.

J. Schoukens, Y. Rolain, and R. Pintelon. Leakage Reduction in Frequency-Response Function Measurements. *IEEE Transactions on Instrumentation and Measurement*, 55(6):2286–2291, 2006. ISSN 0018-9456. doi: 10.1109/TIM.2006.887034.

J. Schoukens, J. Lataire, R. Pintelon, and G. Vandersteen. Robustness Issues of the Equivalent Linear Representation of a Nonlinear System. *2008 IEEE Instrumentation and Measurement Technology Conference*, pages 332–335, May 2008. doi: 10.1109/IMTC.2008.4547056.

J. Schoukens, J. Lataire, R. Pintelon, G. Vandersteen, and T. Dobrowiecki. Robustness Issues of the Best Linear Approximation of a Nonlinear System. *IEEE Transactions on Instrumentation and Measurement*, 58(5):1737–1745, May 2009a. ISSN 0018-9456. doi: 10.1109/TIM.2009.2012948.

J. Schoukens, G. Vandersteen, K. Barbé, and R. Pintelon. Nonparametric Preprocessing in System Identification: a Powerful Tool. *European Journal of Control*, 3-4:260–274, 2009b.

M. Schroeder. Synthesis of low-peak-factor signals and binary sequences with low autocorrelation. *IEEE Transactions on Information Theory*, 16(1):85–89, 1970.

R. J. Schwall, A. M. Bond, and D. E. Smith. On-line fast Fourier transform faradaic admittance measurements: real-time deconvolution of heterogeneous charge transfer kinetic effects for thermodynamic and analytical measurements. *Analytical Chemistry*, 49(12):1805–1812, October 1977. ISSN 0003-2700. doi: 10.1021/ac50020a042.

H.P. Schwan. Electrical properties of tissues and cell suspensions: mechanisms and models. *Proceedings of 16th Annual International Conference of the IEEE Engineering in Medicine and Biology Society*, 1:A70–A71, 1994. doi: 10.1109/IEMBS.1994.412155.

G. Simon and J. Schoukens. Robust broadband periodic excitation design. *IEEE Transactions on Instrumentation and Measurement*, 49(2):270–274, April 2000. ISSN 00189456. doi: 10.1109/19.843062.

D. N. Smith. Tissue impedivity and electro-mathematical modelling of bioimpedances. *Innovation et technologie en biologie et médecine*, 16(6):694–702, 1995. ISSN 0243-7228.

T. Sun, S. Gawad, C. Bernabini, N. G. Green, and H. Morgan. Broadband single cell impedance spectroscopy using maximum length sequences: theoretical analysis and practical considerations. *Measurement Science and Technology*, 18(9):2859–2868, 2007a. ISSN 0957-0233. doi: 10.1088/0957-0233/18/9/015.

T. Sun, D. Holmes, S. Gawad, N. G. Green, and H. Morgan. High speed multi-frequency impedance analysis of single particles in a microfluidic cytometer using maximum length sequences. *Lab on a chip*, 7(8):1034–40, 2007b. ISSN 1473-0197. doi: 10.1039/b703546b.

A. H. Tan and K. R. Godfrey. The generation of binary and near-binary pseudorandom signals: an overview. *IEEE Transactions on Instrumentation and Measurement*, 51(4):pp583–588, 2002.

M. E. Valentinuzzi, J. P. Morucci, and C. J. Felice. Bioelectrical impedance techniques in medicine. Part II: Monitoring of physiological events by impedance. *Critical Reviews in Biomedical Engineering*, 24(4-6):353–466, 1996.

A. van den Bos. Construction of binary multifrequency test signals. In *1st IFAC Symposium on System Identification in Automatic Control Systems*, page Paper4.6, 1967.

A. van den Bos and R. G. Krol. Synthesis of discrete-interval binary signals with specified Fourier amplitude spectra. *International Journal of Control*, 30(5):871–884, 1979.

E. Van Der Ouderaa, J. Schoukens, and J. Renneboog. Peak factor minimization using a time-frequency domain swapping algorithm. *IEEE Transactions on Instrumentation and Measurement*, 37(1):145–147, March 1988. ISSN 00189456. doi: 10.1109/19.2684.

K. Vanhoenacker, T. Dobrowiecki, and J. Schoukens. Design of multisine excitations to characterize the nonlinear distortions during FRF-measurements. *IEEE Transactions on Instrumentation and Measurement*, 50(5):1097–1102, 2001. ISSN 00189456. doi: 10.1109/19.963166.

Part II

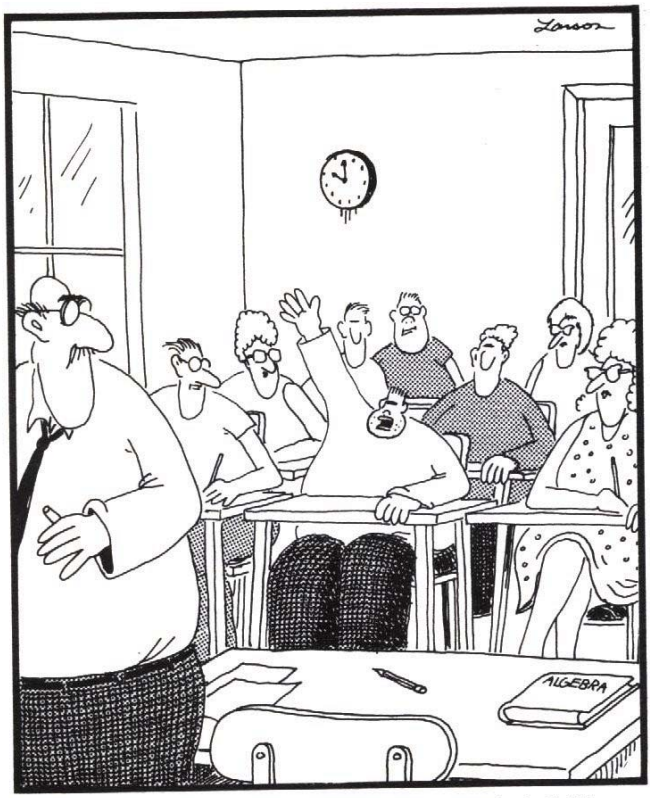

"Mr. Osborne, may I be excused? My brain is full."

The Far Side, by Gary Larson.

This page intentionally left blank.

A

Optimal Multisine Excitation Design for Broadband Electrical Impedance Spectroscopy

This page intentionally left blank.

IOP Publishing Measurement Science and Technology
Meas. Sci. Technol. **22** (2011) 115601 (11pp) doi:10.1088/0957-0233/22/11/115601

Optimal multisine excitation design for broadband electrical impedance spectroscopy

B Sanchez[1], G Vandersteen[2], R Bragos[1] and J Schoukens[2]

[1] Electronic and Biomedical Instrumentation Group, Department of Electrical Engineering, Universitat Politecnica de Catalunya (UPC), Barcelona 08034, Spain
[2] ELEC Department, Vrije Universiteit Brussel (VUB), B-1050, Belgium

E-mail: benjamin.sanchez@upc.edu

Received 14 April 2011, in final form 29 July 2011
Published 13 September 2011
Online at stacks.iop.org/MST/22/115601

Abstract
Electrical impedance spectroscopy (EIS) can be used to characterize biological materials in applications ranging from cell culture to body composition, including tissue and organ state. The emergence of cell therapy and tissue engineering opens up a new and promising field of application. While in most cases classical measurement techniques based on a frequency sweep can be used, EIS based on broadband excitations enables dynamic biological systems to be characterized when the measuring time and injected energy are a constraint. Myocardial regeneration, cell characterization in micro-fluidic systems and dynamic electrical impedance tomography are all examples of such applications. The weakness of such types of fast EIS measuring techniques resides in their intrinsic loss of accuracy. However, since most of the practical applications have no restriction over the excitation used, the input power spectrum can be appropriately designed to maximize the accuracy obtained from the measurements. This paper deals with the problem of designing the optimal multisine excitation for electrical bioimpedance measurements. The optimal multisine is obtained by the minimization of the Cramer–Rao lower bound, or what is the same, by maximizing the accuracy obtained from the measurements. Furthermore, because no analytical solution exists for global optimization involving time and frequency domains jointly, this paper presents the multisine optimization approach partially in both domains and then combines the results. As regards the frequency domain approach, a novel contribution is made for the multisine amplitude power spectrum. In the time domain, multisine is optimized by reducing its crest factor. Moreover, the impact on the information and accuracy of the impedance spectrum obtained from using different multisine amplitude power spectra is discussed, as well as the number of frequencies and frequency distributions. The theory is supported by a set of validation measurements when exciting with the optimal and flat multisine signals and compared to a single frequency ac impedance analyzer when characterizing an RC circuit. *In vivo* healthy myocardium tissue electrical impedance measurements show that broadband EIS based on multisine excitations enable the characterization of dynamic biological systems.

Keywords: broadband electrical impedance spectroscopy, optimal multisine excitation, electrical bioimpedance

1. Introduction

Electrical impedance spectroscopy (EIS) can provide information about electrochemical reactions at interfaces, transport processes in electrolytes and electrical properties of materials. Among the various approaches to EIS experiments, the most common is the application of a single-frequency

ATENCIÓ ¡

Les pàgines 106 a 115 de la tesi contenen la resta de l'article, que no es poden mostrar per decisió de l'editor de la revista.

ATENCIÓN ¡

Las páginas 106 a 115 de la tesis contienen el resto del articulo, però no pueden mostrarse por decisión del editor de la revista.

ATTENTION ¡

Pages 106-115 of the thesis contains the rest of the article, but can not be displayed by decision of magazine editor

Optimal multisine excitation design for broadband electrical impedance spectroscopy B Sanchez *et al* 2011 *Meas. Sci. Technol.* **22** 115601

doi:10.1088/0957-0233/22/11/115601

This page intentionally left blank.

B

Novel Estimation of the Electrical Bioimpedance using the Local Polynomial Method. Application to in-vivo real-time Myocardium Tissue Impedance Characterization during the Cardiac Cycle.

This page intentionally left blank.

Novel Estimation of the Electrical Bioimpedance Using the Local Polynomial Method. Application to *In Vivo* Real-Time Myocardium Tissue Impedance Characterization During the Cardiac Cycle

Benjamin Sanchez*, Johan Schoukens, *Fellow, IEEE*, Ramon Bragos, *Member, IEEE*, and Gerd Vandersteen, *Senior Member, IEEE*

***Abstract*—Classical measurements of myocardium tissue electrical impedance for characterizing the morphology of myocardium cells, as well as cell membranes integrity and intra/extra cellular spaces, are based on the frequency-sweep electrical impedance spectroscopy (EIS) technique. In contrast to the frequency-sweep EIS approach, measuring with broadband signals, i.e., multisine excitations, enables to collect, simultaneously, multiple myocardium tissue impedance data in a short measuring time. However, reducing the measuring time makes the measurements to be prone to the influence of the transients introduced by noise and the dynamic time-varying properties of tissue. This paper presents a novel approach for the impedance-frequency-response estimation based on the local polynomial method (LPM). The fast LPM version presented rejects the leakage error's influence on the impedance frequency response when measuring electrical bioimpedance in a short time. The theory is supported by a set of validation measurements. Novel preliminary experimental results obtained from real-time *in vivo* healthy myocardium tissue impedance characterization within the cardiac cycle using multisine excitation are reported.**

***Index Terms*—Broadband electrical impedance spectroscopy (EIS), electrical bioimpedance (EBI), local polynomial method (LPM), multisine excitation, myocardium tissue electrical impedance.**

I. Introduction

MYOCARDIUM tissue electrical impedance enables the detection of different tissue states. Through animal *in vivo* and *ex vivo* tissue experiments, it has been shown to correlate with many physiological states of the myocardium tissue, such as the regional and global ischemia processes [1], edema [2], and detect humoral-rejection episodes following heart transplantation [3] and [4]. It was proven that the electrical impedance frequency response of the myocardium tissue allows one to distinguish the normal tissue from the ischemic one (loss of blood irrigation after a recent, <3 h, infarction) or from the healed scar, that is the result of an ancient (>1 month) infarction. Electrical impedance characterization of myocardium tissue is usually performed at a single frequency, in the 1–10 kHz range [5] or performing a frequency sweep in the 1 kHz–1 MHz range [1], [6]. Both *in vivo* single-frequency and multifrequency studies have been reported in [5] and for the ischemic tissue [7] and healed scar [4]. The last technique has also been recently applied through a catheter [8].

Measuring the electrical bioimpedance (EBI) steady-state response of a biological time-varying systems, such as the respiratory or cardiovascular systems, is not always interesting, especially when the dynamic behavior itself is pretended to be monitored in real time. Although the time variation of the impedance signal has information about the tissue activity within the cardiac cycle, this information has been usually underestimated in all those studies based on frequency-sweep electrical impedance spectroscopy (EIS). In these cases, the dynamic behavior is usually removed from the impedance signal by means of averaging. In this sense, the most critical situation is the determination of the myocardium tissue state, given that this organ shows the fastest change rates.

To our knowledge, the f rst attempt to characterize the myocardium tissue impedance within the cardiac cycle is dated in 2001 [9]. The acquisition system was based on an arbitrary waveform generator (AWG) (12 bit D/A, 40 Msamples/s) as a signal generator and a digital oscilloscope (500 Msamples/s, 8 bit) as an acquisition system. In this case, the system performance was unable to measure and to process data on the fl because of the limited memory available (only 1 s was recorded) and due to the time needed to transmit data from the oscilloscope to the computer through an IEEE-488 interface. As a result, the system was only able to measure six impedance spectra per second. Moreover, the limited resolution at high frequency did not allow to determine whether there was a spectrum change into the cycle or just a global impedance shift. Nevertheless, the

Manuscript received May 13, 2011; revised July 19, 2011; accepted August 19, 2011. Date of publication; date of current version. This work was supported in part by the Spanish Ministry MICINN SAF2008-05144-C02-02, 080331 from Fundació La Marató de TV3, by the Red de Investigación en Insuficienci Cardiaca (REDINSCOR), by the Fund for Scientifi Research (FWO-Vlaanderen), by the Flemish Government (Methusalem), and by the Belgian Government under the Interuniversity Poles of Attraction (IAP VI/4) Program. *Asterisk indicates corresponding author.*

*B. Sanchez is with the Department of Electronic Engineering, Technical University of Catalonia, Barcelona 08034, Spain (e-mail: benjamin.sanchez@upc.edu).

J. Schoukens and G. Vandersteen are with the Department of Fundamental Electricity and Instrumentation, Vrije Universiteit Brussels, Brussels 1050, Belgium (e-mail: jschouk@irexchange.vub.ac.be; gvanders@irexchange.vub.ac.be).

R. Bragos is with the Department of Electronic Engineering, Technical University of Catalonia, Barcelona 08034, Spain (e-mail: rbb@eel.upc.edu).

Color versions of one or more of the f gures in this paper are available online at http://ieeexplore.ieee.org.

Digital Object Identifie 10.1109/TBME.2011.2166116

Novel estimation of the electrical bioimpedance using the local polynomial method. Application to *in-vivo* real-time myocardium tissue impedance characterization during the cardiac cycle.

Sanchez, B. *et al.* IEEE Transactions on biomedical engineering 2011. Vol 58, núm. 12, p. 3376 - 3385

DOI 10.1109/TBME.2011.2166116

Appendix

Appendix A. Multisine Crest Factor

Consider a real multisine defined by:

$$u(t) = \sum_{n=0}^{N-1} a_n \cos(2\pi f_n t + \varphi_n) \tag{A.1}$$

By definition, the energy of a periodic signal can be found solving the following equation:

$$E_{u(t)} \triangleq \int_{-T_0/2}^{T_0/2} |u(t)|^2 \, dt \tag{A.2}$$

Then, if we replace the signal by the multisine time expression:

$$E_{u(t)} = \int_{-T_0/2}^{-T_0/2} \left| \sum_{n=0}^{N-1} a_n \cos(2\pi f_n t + \varphi_n) \right|^2 dt \tag{A.3}$$

the equation to solve once the quadratic term is expanded is:

$$E_{u(t)} = \int_{-T_0/2}^{T_0/2} \sum_{k=0}^{M-1} \sum_{m=0}^{M-1} a_m a_k \cos(2\pi f_0 t + \varphi_m) \cos(2\pi f_0 t + \varphi_k) dt \tag{A.4}$$

Rearranging the expression using the cosine trigonometric relationship gives:

$$E_{u(t)} = \int_{-T_0/2}^{T_0/2} \sum_{k=0}^{N-1} \sum_{m=0}^{N-1} a_m a_k \frac{\cos(2 \cdot 2\pi f_0 t + \varphi_m + \varphi_k) + \cos(\varphi_m - \varphi_k)}{2} dt \tag{A.5}$$

This allows to simplify equation A.4 into the following expression:

$$E_{u(t)} = 2 \cdot \int_{0}^{T_0/2} \sum_{k=0}^{N-1} a_m^2 \frac{\cos\left(2 \cdot 2\pi f_0 t + 2 \cdot \varphi_m\right) + 1}{2} dt \tag{A.6}$$

At this moment, the summation operator can be moved out of the integral as follows:

$$E_{u(t)} = \sum_{m=0}^{N-1} a_m^2 \int_{0}^{T_0/2} \left(\cos\left(2 \cdot 2\pi f_0 t + 2 \cdot \varphi_m\right) + 1\right) dt \tag{A.7}$$

and the solution is:

$$E_{u(t)} = \sum_{m=0}^{N-1} a_m^2 \left| t + \frac{\sin\left(2 \cdot 2\pi f_0 t + 2 \cdot \varphi_m\right)}{2 \cdot 2\pi f_0} \right|_{0}^{T_0/2} \tag{A.8}$$

Eq. A.8 evaluated at the initial and ending points turns into:

$$E_{u(t)} = \sum_{m=0}^{N-1} a_m^2 \left(\frac{T_0}{2} + \frac{\sin\left(2 \cdot 2\pi f_0 \frac{T_0}{2} + 2 \cdot \varphi_m\right) - \sin\left(2 \cdot \varphi_m\right)}{2 \cdot 2\pi f_0} \right) \tag{A.9}$$

$$E_{u(t)} = \sum_{m=0}^{N-1} a_m^2 \left(\frac{T_0}{2} + \frac{\sin\left(2\pi + 2\varphi_m\right) - \sin\left(2\varphi_m\right)}{2 \cdot 2\pi f_0} \right) \tag{A.10}$$

Eq. A.10 can be simplified because of the *sin* function 2π periodicity into:

$$E_{u(t)} = \sum_{m=0}^{N-1} a_m^2 \left(\frac{T_0}{2} + \frac{\sin\left(2\varphi_m\right) - \sin\left(2\varphi_m\right)}{2 \cdot 2\pi f_0} \right) \tag{A.11}$$

Finally, we obtain that the energy of a real multisine is only function of the number of exciting frequencies N and the norm of the fundamental amplitudes $l_2\left(a\right)$:

$$E_{u(t)} = \frac{T_0}{2} \sum_{m=0}^{N-1} a_m^2 \tag{A.12}$$

By definition, the Crest Factor of an excitation $u\left(t\right)$ is:

$$CF\left(u\left(t\right)\right) = \frac{\left\|u\left(t\right)\right\|_\infty}{\sqrt{\frac{1}{T_0} \int_{-T_0/2}^{T_0/2} \left|u\left(t\right)\right|^2}} \tag{A.13}$$

Rearranging the denominator term using the expression obtained in eq. A.12:

$$CF\left(u\left(t\right)\right) = \frac{\left\|u\left(t\right)\right\|_{\infty}}{\sqrt{\frac{1}{T_0}\frac{T_0}{2}\sum_{m=0}^{N-1} a_m^2}} \tag{A.14}$$

we finally obtain that the Crest Factor for a real multisine excitation is:

$$CF\left(u\left(t\right)\right) = \sqrt{2}\frac{\left\|u\left(t\right)\right\|_{\infty}}{\sqrt{\sum_{m=0}^{N-1} a_m^2}} = \sqrt{2}\frac{\left\|u\left(t\right)\right\|_{\infty}}{\left\|a_m\right\|_2} \tag{A.15}$$

Appendix B. Measuring the Best Linear Approximation (BLA): the Robust Method

The projected input/output spectra of the m^{th} realization and p^{th} period are related to the input/output noise, the Best Linear Approximation, and the stochastic nonlinear distortions as follows:

$$\begin{aligned}
&\overline{U}_R^{[m]}\left(k\right) = \frac{1}{P}\sum_{p=1}^{P} U_R^{[m,p]}\left(k\right) \quad , \quad \overline{Y}_R^{[m]}\left(k\right) = \frac{1}{P}\sum_{p=1}^{P} Y_R^{[m,p]}\left(k\right) \\
&\overline{\sigma}^2_{\overline{U}_R^{[m]}}\left(k\right) = \sum_{p=1}^{P} \frac{\left|U_R^{[m,p]}(k) - \overline{U}_R^{[m]}(k)\right|^2}{P(P-1)} \quad , \quad \overline{\sigma}^2_{\overline{Y}_R^{[m]}}\left(k\right) = \sum_{p=1}^{P} \frac{\left|Y_R^{[m,p]}(k) - \overline{Y}_R^{[m]}(k)\right|^2}{P(P-1)} \\
&\overline{\sigma}^2_{\overline{Y}_R^{[m]}\overline{U}_R^{[m]}}\left(k\right) = \sum_{p=1}^{P} \frac{\left(Y_R^{[m,p]}(k) - \overline{Y}_R^{[m]}(k)\right)\left(U_R^{[m,p]}(k) - \overline{U}_R^{[m]}(k)\right)^*}{P(P-1)}
\end{aligned} \tag{B.1}$$

Additional averaging over the M realizations gives:

$$\begin{aligned}
&\overline{U}_R\left(k\right) = \frac{1}{M}\sum_{m=1}^{M} U_R^{[m]}\left(k\right) \quad , \quad \overline{Y}_R\left(k\right) = \frac{1}{M}\sum_{m=1}^{M} Y_R^{[m]}\left(k\right) \\
&\overline{\sigma}^2_{\overline{U}_R}\left(k\right) = \sum_{m=1}^{M} \frac{\left|U_R^{[m]}(k) - \overline{U}_R(k)\right|^2}{M(M-1)} \quad , \quad \overline{\sigma}^2_{\overline{Y}_R}\left(k\right) = \sum_{m=1}^{M} \frac{\left|Y_R^{[m]}(k) - \overline{Y}_R(k)\right|^2}{M(M-1)} \\
&\overline{\sigma}^2_{\overline{Y}_R\overline{U}_R}\left(k\right) = \sum_{m=1}^{M} \frac{\left(Y_R^{[m]}(k) - \overline{Y}_R(k)\right)\left(U_R^{[m]}(k) - \overline{U}_R(k)\right)^*}{M(M-1)}
\end{aligned} \tag{B.2}$$

and an improved estimate of the input/output noise (co-)variance is given by:

$$\begin{aligned}
&\overline{\sigma}^2_{\overline{U}_R,n}\left(k\right) = \frac{1}{M^2}\sum_{m=1}^{M} \overline{\sigma}^2_{\overline{U}_R^{[m]}}\left(k\right) \quad , \quad \overline{\sigma}^2_{\overline{Y}_R,n}\left(k\right) = \frac{1}{M^2}\sum_{m=1}^{M} \overline{\sigma}^2_{\overline{Y}_R^{[m]}}\left(k\right) \\
&\overline{\sigma}^2_{\overline{Y}_R\overline{U}_R,n}\left(k\right) = \frac{1}{M^2}\sum_{m=1}^{M} \overline{\sigma}^2_{\overline{Y}_R^{[m]}\overline{U}_R^{[m]}}\left(k\right)
\end{aligned} \tag{B.3}$$

Finally, the Best Linear Approximation for the frequency response $\hat{G}_{BLA}(j\omega_k)$, the noise variance $\overline{\sigma}^2_{\overline{G}_{BLA},n}(k)$ and the total variance (including the contribution of the non-linear distortions and noise) $\overline{\sigma}^2_{\overline{G}_{BLA}}(k)$ are found as:

$$
\begin{aligned}
&\overline{G}_{BLA}(j\omega_k) = \frac{\overline{Y}_R(k)}{\overline{U}_R(k)} \\
&\overline{\sigma}^2_{\overline{G}_{BLA},n}(k) = \left|\overline{G}_{BLA}(j\omega_k)\right|^2 \left(\frac{\overline{\sigma}^2_{\overline{Y}_R,n}(k)}{\left|\overline{Y}_R(k)\right|^2} + \frac{\overline{\sigma}^2_{\overline{U}_R,n}(k)}{\left|\overline{U}_R(k)\right|^2} - 2\Re\left(\frac{\overline{\sigma}^2_{\overline{Y}_R\overline{U}_R,n}(k)}{\overline{Y}_R(k)\overline{U}_R(k)^*} \right) \right) \\
&\overline{\sigma}^2_{\overline{G}_{BLA}}(k) = \left|\overline{G}_{BLA}(j\omega_k)\right|^2 \left(\frac{\overline{\sigma}^2_{\overline{Y}_R}(k)}{\left|\overline{Y}_R(k)\right|^2} + \frac{\overline{\sigma}^2_{\overline{U}_R}(k)}{\left|\overline{U}_R(k)\right|^2} - 2\Re\left(\frac{\overline{\sigma}^2_{\overline{Y}_R\overline{U}_R}(k)}{\overline{Y}_R(k)\overline{U}_R(k)^*} \right) \right)
\end{aligned}
\tag{B.4}
$$

List of Figures